To be or not to be an anti-CRISPR: AcrIII-1 and the importance of working with native biological systems

Martínez-Alvarez Laura[1], Stickel Dominic[1], Salegi-Díez Andrea[1], Bhoobalan-Chitty Yuvaraj[1], Peng Xu[1]

[1]Department of Biology, University of Copenhagen, Ole Maaløes Vej 5, 2200 Copenhagen N, Denmark

Correspondence: Xu Peng: peng@bio.ku.dk

ABSTRACT

Viral members of the protein family DUF1874 have been reported to act as anti-CRISPR (acr) proteins that degrade cyclic tetra-adenylate (cA_4), a nucleotide second messenger produced after the activation of several type III CRISPR-Cas systems in bacteria and archaea. Specifically, protein SIRV1 gp29 inhibits type III-A and type III-B CRISPR systems in plasmid-born assays in heterologous systems. In this work, we investigate the function of SIRV1 gp29 and its close homolog SIRV2 gp37 in a native biological context, i.e. in cultures infected by SIRV2. SIRV2 was selected instead of SIRV1 because the latter is not available any more from any laboratories. We demonstrate that gp37 has no anti-CRISPR activity during infection of *Sulfolobus islandicus* LAL14/1 with SIRV2, although it is able to protect SIRV2 from type III targeting when expressed from a plasmid. The inability of gp37 to act as an acr in the native, biological system is due to the protein expression timing: gp37 is a middle/late gene, thus unable to inhibit CRISPR-Cas targeting at the onset of infection. On the other hand, we find that while gp37 is a non-essential gene, it confers a mild replicative advantage to the virus. This advantage is mediated, in hosts with active CRISPR-Cas targeting, by the interaction between gp37 and host protein SiL_1451, which results in the inhibition of the lysine methyltransferase activity of SiL_1451, responsible for extensive methylation of surface lysines of two-thirds of the cellular proteins. Heterologous gene expression from a plasmid-borne non-native promoter has allowed the discovery and characterization of dozens of prokaryotic defense systems in recent years. Although this experimental strategy has several advantages, our study highlights the importance of validating relevant results under native conditions, and the limitations of extrapolating results obtained using heterologous systems.

Keywords: archaeal virus**,** anti-CRISPR, type III CRISPR-Cas, RING nuclease, cyclic tetra-oligoadenylate, lysine methyltransferase

INTRODUCTION

Prokaryotes coexist with a range of mobile genetic elements (MGEs, e.g. viruses, conjugative elements) and consequently have developed multiple systems to control or inactivate them (Doron et al. 2018; L. Gao et al. 2020; L. A. Gao et al. 2022; Vassallo et al. 2022). Among these, CRISPR-Cas constitutes the only known prokaryotic adaptive immunity. Cas proteins, guided by crRNA that is encoded within CRISPR arrays, mediate the cleavage of complementary foreign nucleic acids (Makarova et al. 2020). CRISPR-Cas systems are divided in two classes, each containing three types (I, III and IV for class 1 and types II, V, VI for class 2) that are further subdivided into several subtypes (Makarova et al. 2020). Among the diverse systems, type III are particularly interesting because base-paring of the crRNA with the target RNA elicits specific target degradation by the Cas7-backbone and activates the Cas10 subunit, which in turn degrades DNA non-specifically via its nuclease HD domain (Samai et al. 2015; Peng et al. 2015; Kazlauskiene et al. 2016) and synthesizes cyclic oligoadenylates (cA) via its Palm domain (Han et al. 2018; Kazlauskiene et al. 2017; Niewoehner et al. 2017). The cyclic oligonucleotide messengers amplify the type III immune response through the activation of CRISPR-Cas associated proteins critical for robust immunity (Deng et al. 2013; Foster et al. 2019; Hatoum-Aslan et al. 2014; Han, Pan, et al. 2017; Rostøl and Marraffini 2019; Jiang, Samai, and Marraffini 2016), such as Csx1 in *Saccharolobus islandicus* (previously *Sulfolobus islandicus*), a non-specific RNase activated by cyclic tetra-adenylate (cA_4) produced by its subtype III-B CRISPR-Cas system (Han, Pan, et al. 2017; Han, Li, et al. 2017).

Accordingly, viruses possess strategies to counteract cellular defenses and a mechanism to inhibit CRISPR-Cas systems involves anti-CRISPR proteins (Acrs), of which two were reported to work in the evasion of type III CRISPR-Cas targeting. AcrIIIB1 is found in archaeal viruses of the Ligamenvirales order and is required for rudivirus SIRV2 to circumvent *S. islandicus* type III-B immunity through binding to the host type III-B effector complex (Bhoobalan-Chitty et al. 2019). The other type III inhibitor, AcrIII-1, is widespread in prokaryotic viruses and its RING nuclease activity rapidly and specifically degrades cA_4, thus being able to neutralize type III subtypes that synthesize this nucleotide messenger (Athukoralage et al. 2020). Importantly, the activity of the AcrIII-1 family was characterized in heterologous systems using the *acrIII-1* member SIRV1 *gp29* expressed from a plasmid (Athukoralage et al. 2020). While rudivirus isolate SIRV1 is no longer available in any laboratories, its closest relative SIRV2 (87.27% average nucleotide identity and thus corresponding to the same viral species) encodes an AcrIII-1 homolog (SIRV2 gp37) with 85% amino acid identity. In this work, we investigate the role of the AcrIII-1 homolog SIRV2 gp37 during SIRV2-infection of its host *S. islandicus* LAL14/1 and demonstrate that gp37 does not exert Acr activity primarily due to having a late expression pattern. However, gp37 is a multi-functional protein capable of

interacting with cellular protein lysine methyltransferase and hereby conferring a mild replication advantage unrelated to its RING nuclease activity. Yet, the ability to cleave cA_4 becomes relevant in the absence of type I-A CRISPR-Cas targeting, implying a physiological role of this second messenger independent to its so far reported function in CRISPR adaptive immunity. These findings can be extrapolated to SIRV1 gp29, as it shares identical genomic neighborhood and regulation as SIRV2 gp37. While plasmid-based heterologous systems have been essential for the discovery and characterization of novel defense mechanisms and their anti-defense counterparts (Doron et al. 2018; L. Gao et al. 2020; L. A. Gao et al. 2022; Vassallo et al. 2022; Uribe et al. 2019; Forsberg et al. 2019; Watters et al. 2018; Marino et al. 2018), our results highlight the importance of using native biological systems to confirm the function of newly characterized defense and anti-defense systems.

MATERIALS AND METHODS

Strains and growth conditions. Strains of *S. islandicus* LAL14/1 Δarrays, Cmr-α and $\Delta Cas6_{(I-D)}$ (Supplementary Table 1) were grown in basic salts medium (Zillig et al. 1993) supplemented with 0.2% sucrose, 0.2% casamino acids, vitamin mixture and 0.002% uracil (SCVU medium) at 78°C with agitation. Uracil was removed from the medium composition after plasmid complementation of the ΔpyrEF deletion. Inducible expression of mini-CRISPR arrays, protein expression or knockdown cassettes was achieved by addition of 0.2% D-arabinose. Strains of *Escherichia coli* NEB Stable (NewEngland Biolabs) or Rossetta (DE3) were used for plasmid cloning and protein expression, respectively and grown in LB medium supplemented with antibiotics. Cellular and viral strains used in this work are listed in Supplementary Table 1.

Virus propagation and quantification. Cultures of *S. islandicus* LAL14/1 Δarrays at OD_{600} of 0.2 were infected with the desired virus strain (multiplicity of infection or MOI between 0.01-0.001) and cell turbidity was monitored until a decrease in optical density was observed (around 48 hours post-infection). Cell debris was removed by centrifugation at 10 000 x g, 15 min and virus present in the supernatant was determined by plaque assay as described previously (Mayo-Muñoz et al. 2018). Two milliliters cells OD 0.2 were mixed with serial dilutions of the supernatant and incubated at 78°C for 30 min, then mixed with 2 mL pre-warmed 0.4% Gelzan (Merck) and immediately plated on pre-warmed SCVU-0.7% gelzan plates. Plates were tightly closed and incubated in a plastic box at 78°C for around two days. Average nucleotide identity (ANI) between SIRV1 and SIRV2 were calculated using the ANI calculator tool from the enveomics collection (http://enve-omics.ce.gatech.edu/).

Infection of cell cultures. Triplicate cultures of the appropriate *S. islandicus* strain were infected at OD_{600} 0.1 with the corresponding virus at the MOI indicated for each experiment and culture growth curves were determined by measuring the absorbance at 600 nm at regular time-points. One-milliliter samples were taken at the indicated time-points to quantify virus in the supernatant as described above.

Plasmids, oligonucleotides and DNA sequencing. Plasmids and oligonucleotides used in this work are listed in Supplementary Tables 2-3. Oligonucleotide synthesis was carried out by Integrated DNA Technologies, Inc. Sanger sequencing used for construct verification was done by Eurofins Genomics.

Plasmid construction. Polymerase chain reactions for cloning were carried out using Phanta Max Super-Fidelity DNA polymerase (Nanjing Vazyme Biotech Co. Ltd). PCR reactions for colony screening and verification of mutants were done using Taq DNA polymerase (Thermo Scientific) For expression of proteins in *E. coli*, genes were PCR amplified from *S. islandicus* LAL14/1 or SIRV2 genomic DNA with the corresponding primers and inserted in the MCS of vectors p15AIE, pET30 or pETDuet (Supplementary Tables 2-3). For expression of proteins in *S. islandicus*, genes were PCR amplified and cloned into pEXA3. For constructions of virus strains we employed CRISPR-based genetic editing method (Mayo-Muñoz et al. 2018). The corresponding protospacer was cloned into the mini-CRISPR array of the pGE-based vectors and suitable donor DNA for homologous recombination was inserted at the indicated restriction sites. Knockdown plasmid was constructed by inserting a subtype I-A protospacer targeting SiL_1451 into pGE1. Efficiency of silencing was determined by RT-qPCR and through the determination of protein methylation levels by western blot. Alanine screening mutants of gp37 and SiL_1451 were constructed through site-directed mutagenesis (Zheng, Baumann, and Reymond 2004) using the corresponding primers in Supplementary Table 3.

Cyclic oligoadenylate cleavage assays. Cyclic oligoadenylate was generated as described previously (Han et al. 2018). Briefly, around 40 nM Cmr-α complex containing only crRNA SS1 targeting the *lacS* gene was mixed with 100 nM target RNA SS1-46, approximately 1 nM α^{32}ATP (Perkin Elmer Waltham), 0.1 mM cold ATP, 10 mM Mn^{2+}, 5 mM DTT and 20 mM MES pH 6, and incubated at 70°C for 30 min, followed by heat-inactivation at 95°C for 5 min. For single turnover kinetics, 4 μM protein and cOA mix (1:40 ratio) were incubated in 20 mM MES pH 6 and 10 mM Mn^{2+} in 20 uL reactions. Samples were incubated at 70°C for the indicated times and cleavage reaction was stopped by the addition of phenol:chloroform (Thermo Scientific) in a 1:1 ratio. The aqueous phase was recovered and cOA degradation was visualized by electrophoresis in 24% urea-polyacrylamide gels in TBE buffer, followed by phosphor imaging with a Typhoon FLA 700 (GE Healthcare). Kinetic analysis was done as

described previously (Athukoralage et al. 2020), quantifying cOA_4 using ImageJ (Schneider, Rasband, and Eliceiri 2012) and fitting the data to a single exponential curve (y=m1 + m2*(1-exp(-m3*x)); m1=0.1, m2=1 and m3=1) using GraphPad Prism version 9.4.1 (681). Raw data for kinetic analysis are available in Supplementary Table 4.

Construction of SIRV2 strains. Overnight cultures of *S. islandicus* Δarrays harboring the corresponding genome-editing plasmid were infected with the corresponding parental virus at an MOI of 0.1 and incubated overnight. Virus present in the supernatant was collected by centrifugation at 4000 x g for 5 min and 10 μL of the supernatant were used to infect a fresh culture. The process was repeated until the desired virus strain could be detected by PCR (oligonucleotides are listed in Supplementary Table 3). Virus mutants were finally purified through plaque assay.

Time-course of virus infection. *S. islandicus* cultures were grown to an optical density of 0.1-0.2 and infected with the corresponding SIRV2 strain at the indicated multiplicity of infection. Growth was monitored to up to 72 h by measuring OD_{600} and culture samples taken at different time-points to determine virus in the supernatant or for western-blot analysis.

Protein expression and purification. Constructs were transformed into *E. coli* Stable cells and plasmid sequence was verified through Sanger sequencing. For protein expression in *E. coli*, plasmids were transformed into Rossetta (DE3) competent cells and 0.5 L of culture were grown in LB medium at 37°C until OD600 reached 0.8, when protein expression was induced by addition of 0.3 mM isopropyl-1-thio-β-D-galactopyranoside (IPTG) and cells were grown at 18°C overnight before harvesting through centrifugation at 10 000 x g for 10 min, resuspended in the appropriate lysis buffer and stored at -80°C until purification. Samples expressing gp37 or gp29 were resuspended in gp37-lysis buffer (50 mM Tris-HCl pH 8, 200 mM NaCl, 5% (v/v) glycerol and 30 mM imidazole), while purification of SiL_1451 and Cren7 was done as described previously (Chu et al. 2012; L. Guo et al. 2008). For protein expression in *S. islandicus*, plasmids were electroporated into the corresponding strain as described previously (Mayo-Muñoz et al. 2018). The desired volume of culture (starting OD_{600} 0.05) was grown at 78°C under agitation and protein expression was induced through the addition of 0.2% D-arabinose to the medium and cells were collected at OD600 around 0.8 by centrifugation, resuspended in the appropriate lysis buffer and stored at -80°C. For lysis of cells, samples were thawed, sonicated (30 cycles of a 3 s pulse plus a 3 s pulse off) and lysed using a French press (FPG 12800, Homogeneising systems LTD). Lysates were clarified of cell debris by two rounds of centrifugation at 12 500 x g for 30 min at 4°C and filtered using a nitrocellulose syringe filter (0.45 μm pore size). His-tagged proteins were purified using HisTrap HP columns

(Cytiva). Hemagglutinine-tagged proteins were purified using anti-HA agarose (Thermo Scientific™). Fractions were pooled and concentrated using ultrafiltration units Protein Concentrator PES (3 kDa MWCO) (Pierce™) and loaded onto a Superdex 75 10/300 GL column. Samples of gp37 and gp29 were eluted in gp37-FPLC-buffer (50 mM Tris-HCl pH 8, 200 mM NaCl and 5% (v/v) glycerol). Protein purification was monitored using 12% SDS-PAGE and protein concentration was determined with the Qubit™ protein assay (Thermo Fisher Scientific, catalog no.Q33211).

Pull-down of N-terminal HA-tagged gp37. To purify the gene product of *gp37* and any potential interaction partners, 12 L of *S. islandicus* Δarrays were grown to OD_{600} 0.2 and infected with SIRV2M N-HA-gp37 engineered to express a N-terminal hemagglutinin tagged gp37 (MOI 0.5-1) and incubated for 3 h at 78°C under agitation. Cells were recovered through centrifugation at 10 000 x g for 10 min and the pellet was resuspended in TBS buffer (20 mM Tris HCl pH 7.6 and 150 mM NaCl). Protein was purified using purified anti-HA agarose (Thermo Fisher Scientific) as described above and fractions were analyzed by SDS-PAGE. A fraction containing gp37 and co-purifying protein was analyzed by liquid chromatography-mass spectrometry using the commercial service of Alphalyse, Denmark.

Western blot and antibodies. For western blot analysis of uninfected and infected cell extracts, cells from samples of approximately 15 mL were recovered by centrifugation at 10 000 x g, 1 min and resuspended in 2 mL WB lysis buffer (25 mM Tris-HCl pH 7.5, 150 mM NaCl, 1 mM EDTA, 0.1% Triton). Cell lysis was achieved through 15 cycles of sonication (3 s pulse on and 3 s pulse off). Total cell extracts or fractions from protein purification were resolved on 12% SDS-PAGE and transferred to a nitrocellulose membrane using a TransBlot® semi-dry transfer unit (Bio-Rad Laboratories, Inc) and transfer buffer (48 mM Tris base, 39 mM glycine, 10% EtOH, 0.05% Tween 20) at 15 V for 30 min. The membrane was blocked with TBS-0.5% Tween 20 (TBST) buffer with 5 % skimmed milk or 0.5% bovine serum albumin (BSA, for the detection of lysine methylation) for 30 min at room temperature and incubated overnight at 4°C in TBST with 1% skimmed milk or BSA and the corresponding primary antibody. The membrane was washed with TBS, followed by a 1 h incubation at room temperature in TBST-1% skimmed milk/BSA and the corresponding secondary antibody (1:10 000 dilution) and washed with TBS. Finally, the SuperSignal™ West Pico Plus Chemiluminiscent Substrate (Thermo Fisher Scientific) was used for detection via chemiluminiscence. The rabbit anti-gp37 polyclonal antibody was produced by Innovagen AB (Sweden) using recombinant C-terminally His-tagged gp37 expressed in *E. coli* and purified as described above. The rabbit polyclonal antibodies anti-gp17, anti-gp48 and anti-aIF2β were described previously (Martínez-Alvarez, Deng, and Peng 2017; Bhoobalan-Chitty et al. 2019; Märtens et al. 2014) and used in a 1:10

000 dilution. The monoclonal HA-epitope tag antibody 2-2.2.14 (Invitrogen, catalog no. 26183) was used for detection of hemagglutinin-tagged proteins (1:5000 dilution). The rabbit polyclonal antibody to methylated lysines (Abcam, catalog no. ab23366) was used for the detection of protein methylation levels (dilution 1:5000). The secondary antibodies goat anti-mouse IgG (H+L) HRP (Thermo Scientific, catalog no. 32430) and goat anti-rabbit IgG-peroxidase (Sigma-Aldrich, catalog no. A0545) were used in a 1:10 000 dilution.

RNA extraction, cDNA synthesis and real-time quantitative PCR (RT-qPCR). Samples of the control strain *S. islandicus* LAL14/1 Δarrays pGE1 and the SiL_1451-knockdown strain *S. islandicus* LAL14/1 Δarrays KD.SiL_1451 were grown in medium supplemented with 0.2% arabinose for approximately 12 h before cell recovery through centrifugation. RNA was extracted using TRI reagent (Sigma-Aldrich, catalog no. 93289) and DNase I-treated (Thermo Fisher Scientific, catalog no. EN0525) according to the instructions of the manufacturers. After verification of RNA integrity through gel electrophoresis, cDNA synthesis was carried out using RevertAid RT reverse transcription kit using random hexamers (Thermo Fisher Scientific, catalog no. K1691), including reactions without reverse transcriptase as controls to discard DNA contamination. RT-qPCR was done using the PowerUP SYBR Green mastermix (Applied Biosystems, catalogue no. A25742) as recommended by the provider for a 10 μL reaction volume and 2 μL diluted cDNA (1:10 dilution). Reactions were amplified on a Quant Studio 3 (Applied Biosystems) with the following program: 50°C for 2 min, 95°C for 2 min and 40 cycles of 95°C for 15 s followed by 58°C for 1 min. Primers used to amplify SiL_1451 and 16S rRNA (used as reference) are described in Supplementary Table 3. The results correspond to the data from three biological samples with three technical replicates each and the SiL_1451 relative level of expression in the knockdown strain KD.SiL_1451 with respect to the control strain was calculated using the threshold cycle (ΔC_T) method (Livak and Schmittgen 2001). The C_T values of samples and standard curves are reported in Supplementary Table 5.

Methyltransferase assay. In vitro methyltransferase activity was measured using the MTase-Glo™ methyltransferase assay (Promega, catalog no. V7601) following the protocol of the manufacturer, with 50 μL reactions carried out in white, opaque flat-bottom OptiPlate-96 microplates (Perkin-Elmer, catalog no. 6005290) at 50°C for 30 min in SiL_1451-MTase buffer (20 mM Tris pH 8, 50 mM NaCl, 1 mM EDTA, 3 mM $MgCl_2$ and 0.1 mg/mL BSA) using 10 μM S-adenosyl-L-methionine (SAM), 0.5 μM SiL_1451 purified enzyme and 8 μM recombinant Cren7 as substrate. To test the effect of gp37 over the methyltransferase activity of SiL_1451 the substrate concentration used was 4 μM Cren7 and 4 μM gp37. Incubations with MTase-Glo Reagent and Detection solution were done at room temperature for 30 min, according to

the manufacturer instructions. Luminiscence was measured using a FLUOstar® Omega (BMG-Labtech) plate-reading luminometer.

Structural models. The structure of the gp37:SiL_1451 complex was predicted using AlphaFold2 (Jumper et al. 2021). As gp29 is reported to be a dimer (Athukoralage et al. 2020) and SiL_1451 is a monomer (Chu et al. 2016), a dimeric conformation for gp37 was used to model the interaction with a monomeric SiL_1451.

Virus competition assays. The indicated viruses for each experiment were mixed in a proportion 1:1 and the virus mix was used to infect cultures of the strains of *S. islandicus* ΔCas6$_{(I\text{-}D)}$ and ΔCas6$_{(I\text{-}D)}$.KD.SiL_1451 with an MOI of 0.01, or the strains Δarrays, Δarrays.KD.SiL_1451, Δarrays_OFFspacer (Δarrays pGE1.IASIRV2gp38.sp), Cmr-α targeting (Cmr-α pC$_{gp39}$) and I-A targeting (Δarrays pGE1.IASIRV2gp03.noPAM.sp) with an MOI of 0.001, all at an initial OD_{600} of 0.1. Cell density was monitored regularly for 2-4 days until cell death was evident by a decrease in absorbance, at which point 1 mL culture samples were taken and centrifuged at 10 000 x g for 1 min to recover the virus present in the supernatant. This corresponds to a single virus transfer step. To start a new transfer, a 10^{-4} (for Δarrays-based strains) or a 10^{-3} (for ΔCas6$_{(I\text{-}D)}$-based strains) dilution of the virus supernatant was used to infect a fresh culture of the same strain (initial OD_{600} of 0.1) and processed as described before. Between 6-12 transfers were carried out as indicated for each particular experiment. Presence of each virus strain in the supernatant was determined by PCR using Taq polymerase (Thermo Scientific) and 20 μL reactions containing 1 μL of virus supernatant. The oligonucleotides Dgp37.check.F and Dgp37.check.R were used to detect SIRV2M (wild-type strain) and SIRV2Δgp37 (gp37 knock-out) using the following program: 95° for 1 min, 25 cycles of 95°C for 15 s, 58°C for 15 s and 72°C for 1 min. The oligonucleotides Check.dgp37.F and Check.gp37.R were used for the detection of SIRV2dgp37 (dead gp37), while Check.gp37wt and Check.gp37.R were used for the detection of SIRV2M with the following program: 95°C for 1 min and 25 cycles of 95°C for 15 s, 58°C for 15 s and 72°C for 15 s. The presence/absence of a virus in the supernatant was determined by the presence of a band of the corresponding PCR product visualized with gel electrophoresis.

RESULTS

AcrIII-1 homolog gp37 of SIRV2 is unable to inhibit CRISPR-Cas III-B immunity during infection of the host *S. islandicus* LAL14/1

Previous work characterizing members of the AcrIII-1 family showed that the plasmid-borne gp29 encoded by the archaeal rudivirus SIRV1 conferred protection to an *acrIII-1*-null virus SSeV in the presence of CRISPR-Cas III-B immunity (Athukoralage et al. 2020). The results by Athukoralage et al. (2020) were of particular interest to us given that a SIRV2 mutant lacking *acrIIIB1* (*gp48*) but carrying *acrIII-1* (*gp37*) was highly sensitive to CRISPR-Cas type III-B interference (Bhoobalan-Chitty et al. 2019), suggestive of no AcrIII activity derived from the SIRV2 *acrIII-1*. SIRV2 is closely related to SIRV1 at the core genome region (87.27% average nucleotide identity) and the two viral genomes share high similarity at the amino acid level and genomic organization (Fig. 1A). Moreover, SIRV2 gp37 is 85% identical to SIRV1 gp29 at the amino acid level (Fig. 1B). To understand the discrepancy of AcrIII-1 activity between the two works, we set on to investigate the role of SIRV2 gp37 during infection. We selected SIRV2 as our model system because the SIRV1 isolate is no longer available in any laboratories.

We first compared the ability of the two rudiviral AcrIII-1 homologs to degrade cA_4 and found that the catalytic rate of SIRV2 gp37 is 50-60% lower than that of SIRV1 gp29 (Fig. 1C). This difference is mainly attributable to a different residue in the catalytic site (a polar residue S49 of SIRV1 gp29 vs. a hydrophobic residue A49 in SIRV2 gp37), as introducing the single change A49S in gp37 increased the catalytic rate of the protein (Fig. 1C).

We then investigated the capacity of AcrIII-1 to protect SIRV2 from type III targeting in its host *Saccharolobus islandicus* LAL14/1. We constructed viral knock-out mutants of *acrIIIB1* (*gp48*) and *acrIII-1* (*gp37*) and assessed their ability to infect a strain of *S. islandicus* LAL14/1 with active III-B CRISPR targeting. Only viruses encoding *acrIIIB1* are able to lyse the host and replicate to high titer, while deletion of *acrIII-1* showed around a 3-fold decrease in the production of viral progeny (from 2.9×10^8 to 7.3×10^7 PFUs/mL) (Fig. 1D).

Athukoralage et al. showed that plasmid-borne SIRV1 gp29 protected virus SSeV from the type III CRISPR defense of *S. islandicus* M.16.4 (Athukoralage et al. 2020). We reasoned that protein expression from a plasmid might have traits that allow for effective inhibition of type III CRISPR-Cas activity. To test this, we infected cells that express SIRV1 gp29 or SIRV2 gp37 from a plasmid with a virus lacking both *acrIIIB1* and *acrIII-1* (SIRV2 Δacrs). In agreement with the results described by Athukoralage et al., plasmid-borne expression of gp29 homologs is enough to abrogate type III targeting and allows for efficient virus replication (Fig. 1F). This result proves that the ring nuclease activity, when expressed from a plasmid, can protect infecting viruses from type III CRISPR-Cas immunity.

Middle/late expression of the RING nuclease proteins from the viral genome makes them unable to inhibit type III CRISPR-Cas targeting

Rudiviruses exhibit a genomic organization where functionally related genes appear to cluster together, with anti-defense genes located at the termini of the genome and capsid proteins encoded at the middle (Fig. 2A). The RING nuclease homologs in SIRV1 and SIRV2 are part of a four-gene operon located in the middle of the genome (Fig. 2A). The other three genes of the operon encode rudiviral core proteins (Mayo-Muñoz et al. 2018) and include the viral Holliday junction resolvase thought to be involved in genome maturation and packaging (Birkenbihl et al. 2001). The whole operon exhibits the transcription pattern of middle/late genes (Quax et al. 2013). Given that the promoter of the operon has a nearly-identical sequence in both viruses (Fig. 1B), we assume that SIRV1 gp29 is also a middle/late gene.

We hypothesized that the absence of type III Acr activity of the native gp37 could be due to its late expression pattern. Western blot of lysates from SIRV2-infected cultures show that, while early gene products such as AcrIIIB1 can be detected as early as 30 minutes post-infection, middle/late gene products like gp37 and gp17 (a ssDNA-binding protein involved in viral genome replication (Y. Guo et al. 2015)) are detected at 2 hours post-infection (Fig. 2B).

To explore if it is the expression timing or the expression level that impedes gp37 to act as an Acr during SIRV2 infection, we compared the protein level of plasmid-borne gp37 and viral-encoded gp37. The expression level of gp37 is, on average, 20% higher in SIRV2-infected cells at 6 hpi than that of plasmid-borne gp37 (Fig. 2C), showing that protein levels during infection would have otherwise been enough to achieve the Acr activity. To further confirm that expression timing is important for the biological function of the viral RING nuclease proteins, we constructed a virus strain lacking *acrIIIB1* and encoding SIRV1 gp29 under the control of an arabinose inducible promoter (SIRV2-*Paragp29*) (Fig. 2D). Without induction, SIRV2-*Paragp29* is unable to replicate (Fig. 2E, left panel), but induction of gp29 at the onset of infection partially recovers the ability of SIRV2 to infect its host (Fig. 2F) and allows SIRV2-*Paragp29* to reach comparable titers to those of the parental virus (Fig. 2F). Taken together, these results demonstrate that early expression of the viral RING nuclease proteins is required for them to exert Acr activity, explaining why SIRV2 gp37, and probably SIRV1 gp29, cannot inhibit type III CRISPR immunity in a natural setting.

SIRV2 gp37 interacts and inhibits the host lysine methyltransferase SiL_1451

To investigate the biological function of gp37, which is not a type III CRISPR inhibitor, we looked for interaction partners of the protein during virus infection. We performed a pull-down experiment using an N-terminally HA-tagged gp37 encoded within the viral genome, thus the assay was performed in SIRV2-infected cultures where expression regulation of gp37 follows the native biological conditions. The recombinant SIRV2 HA-gp37 had similar infectivity to the

parental strain (Fig. S1), demonstrating that the tag does not affect the infectivity of the virus. A single additional band over the 15 kDa marker position was detected by SDS-PAGE and mass spectrometry showed it to match the 18 kDa host protein lysine-methyltransferase SiL_1451 (Fig. 3A and Fig. S2). The interaction between the two proteins was confirmed with a complementary pull-down assay performed using a C-terminally tagged SiL_1451 expressed from a plasmid, which recovered gp37 from SIRV2-infected cells (Fig. 3B). The yield and the purity of SiL_1451-HA is very low despite arabinose induction of gene transcription, and protein identity was thus confirmed using western blot (Fig. 3B, bottom).

SiL_1451 is known to mediate extensive protein lysine methylation with broad substrate specificity, being responsible for the mono-methylation of one-third of all proteins encoded by *S. islandicus,* including several of the most abundantly expressed proteins (Chu et al. 2012; Ea et al. 2016). Post-translational lysine methylation is widespread in the crenarchaeota, albeit the functional significance of this modification is yet to be elucidated (Chu et al. 2016). To investigate if the interaction between gp37 and SiL_1451 affects the enzymatic activity of the latter, we determined the levels of intracellular protein methylation in cells carrying a plasmid-borne gp37 by western blot using a polyclonal antibody recognizing mono- and di-methylated lysines. We observed a drastic reduction of 80% in protein methylation levels after induction of gp37, indicating that gp37 inhibits SiL_1451 (Fig. 3C).

To get further insight into the mechanism by which gp37 inhibits the methyltransferase activity of SiL_1451, a model of the interacting proteins was first predicted by Alphafold2 (Fig. 3D). Several contacts are predicted between one chain of the gp37 dimer and the N-terminal and C-terminal ends of SiL_1451, including ionic interactions between D28, R29 and D59 in gp37, and L142, E129 and R133 in SiL_1451, as well as hydrophobic and polar interactions mediated by residues L30, L98, Y101 and E102 in gp37 and P8, V10, P102, L104 and M148 of SiL_1451 (Fig. 3D). A comparison of the conformation of SiL_1451 in our model to the crystal structures of the methyltransferase in the open (cofactor-binding SiL_1451-SAM) and closed (reaction product-binding SiL_1451-SAH) conformations suggests that the interaction with gp37 positions SiL_1451 in a closed conformation where access to the methyltransferase active site is blocked by the placement of the N-terminal portion of the protein (Fig. 3E). If gp37 locks SiL_1451 into an inactive conformation, this could explain the lack of methyltransferase activity observed in the presence of gp37 (Fig. 3C).

The gp37-SiL_1451 model was tested through an alanine-scanning of the presumed interacting residues. We focused on the residues putatively mediating the contact between the two proteins while maintaining their respective catalytic activities. For this, we determined the ring nuclease activity and methyltransferase activity of gp37 and SiL_1451, respectively,

and selected the mutants exhibiting activity comparable to the wild-type proteins (Fig. S3). We included as controls the catalytically inactive gp37 H47A and SiL_1451 D34A, previously shown to abrogate cA4 cleavage and lysine methyltransferase activity, respectively (Athukoralage et al. 2020; Chu et al. 2016). Mutation of the gp37 residues D28, R29, L98 and E102 did not impair cA4 degradation, and only M148 mutation in SiL_1451 maintained wild-type-like lysine methylation capacity, while K104 and E129 show halved enzymatic activity (Fig. S3).

We were not able to reproduce the SiL_1451-gp37 interaction *in vitro,* nor could we identify any alteration in protein activity due to the presence of the putative interaction partner. Therefore, we evaluated the interaction capacity of the gp37 mutants through pull-down assays in *S. islandicus* cells expressing plasmid-borne gp37 with a histidine tag attached to the C-terminus. The wild-type and catalytically dead gp37 positive controls co-purify together with SiL_1451, as indicated by the presence of a 18 kDa band corresponding to the lysine methyltransferase (Fig. 3F). This band is missing in all the alanine-mutants tested, indicating an impaired interaction with SiL_1451 (Fig. 3F). To test the gp37-interaction capability of the SiL_1451 mutants, pull-down assays were carried out using a plasmid-expressed N-terminally His-tagged SiL_1451 together with an untagged gp37 cassette. Although SiL_1451 has similar low yields as previously seen (Fig. 3B), the wild-type protein co-purifies with gp37, while the catalytically dead mutant D34 and mutant E129 appear both to have a decreased interaction with gp37. On the other hand, mutant M148 shows the greatest reduction in gp37 co-purification, as the 14 kDa band corresponding to gp37 is barely visible (Fig. 3G). Overall, the results demonstrate that all the tested residues are involved in the physical interaction between the two proteins. Interestingly, a decrease in lysine methylation levels was detected in the lysates of all the gp37 mutants tested in these assays, comparable to the level of methylation in cells expressing the wild-type proteins (Fig. 3H). These results suggest that a single mutation of the residues mediating the gp37-SiL_1451 binding may not be enough to completely abrogate the interaction between gp37 and SiL_1451. An alternative explanation is that the low protein level of SiL_1451 is readily inhibited by the high intracellular level of gp37, even if the interaction between the two is impaired.

SIRV2 gp37 is a multi-functional protein that confers a mild replicative advantage through different mechanisms

gp37 was shown to confer a mild replicative advantage in *Sulfolobus* carrying CRISPR type III-B immunity, as Δ*gp37* exhibits a reduction of around 3-fold in infectivity when compared to the parental virus (Fig. 1D). Moreover, this replicative advantage is maintained during infection

of a strain without CRISPR-Cas defense (Fig. 4A), suggesting that it is independent of the CRISPR immunity.

To explore the roles of the ring nuclease activity of gp37 and its interaction with SiL_1451 lysine methyltransferase in the gp37-mediated replicative advantage, we constructed the virus strain SIRV2 d*gp37* that encodes the inactive ring nuclease variant gp37 H47A, and confirmed that the expression level of dead gp37 is comparable to that of the wild-type protein (Fig. S4). Additionally, we constructed *SiL_1451* knockdown strains of *S. islandicus* achieving a 60% reduction of the *SiL_1451* mRNA and a decrease of ~ 50% in the intracellular lysine methylation level (Fig. S5).

Next, we performed competition assays between the parental and the recombinant SIRV2 strains Δ*gp37* (without gp37) or d*gp37* (with abrogated cA_4 cleavage activity). Viruses were mixed in a 1:1 ratio and used to infect different *S. islandicus* strains at low multiplicity of infection (0.001-0.0001). When complete lysis of the culture was achieved, culture supernatants containing extracellular virus were used to infect fresh cultures for a “transfer” step. This process was repeated for 6-12 transfers and the presence of each virus strain was assessed using qualitative PCR.

In both cells with active CRISPR-Cas targeting or no targeting, SIRV2 Δ*gp37* is quickly out-competed by the parental strain after 2-3 transfers (Fig. 4B and 4C, top panels). However, the disadvantage of lacking gp37 is sensibly neutralized after silencing of SiL_1451, where SIRV2 Δ*gp37* is still detectable in the supernatant after twelve transfers (Fig. 4B and 4C, bottom panels). This suggests that gp37 confers a replicative advantage primarily through its ability to inhibit SiL_1451 and this advantage is independent of CRISPR immunity.

We then explored the role of ring nuclease activity during infection by the competing parental and dgp37 viruses. The advantage of the parental virus was minimal in cells carrying CRISPR I-A and III-B immunities, with dgp37 persisting after twelve transfers (Fig. 4D).

However, the ring nuclease activity is critical to the gp37-mediated replicative advantage in cells carrying no CRISPR immunity, as SIRV2 dgp37 rapidly disappeared from the population after two transfers (Fig. 4E), contrary to what occurred in cells with CRISPR immunity. The CRISPR-null strain lacks any CRISPR arrays, but contains fully functional subtype I-A and III-B *cas* gene cassettes (He et al. 2018). We then selectively activated each of the CRISPR-Cas subtypes by providing a spacer for their specific activation. Virus d*gp37* was out-competed quickly by the parental virus in the control strain carrying a spacer not matching the viral genome, as well as in the strain with subtype III-B targeting (Fig. 4F, first and second panels).

However, dgp37 disadvantage was abated in the strain with active I-A targeting (Fig. 4F, third panel), signifying that I-A CRISPR-Cas targeting reduces the need for cA_4 cleavage or somehow inhibits the ring nuclease activity.

In both host strains with and without CRISPR immunity, *SiL_1451* knockdown does not alter the phenotype of the competition between the parental and the dgp37 viruses (Fig. 4D and 4F, bottom panels), in contrast to what was observed in the competition assays between the parental and Δgp37 viruses. The results imply that gp37 confers mild replicative advantage through at least two pathways. The first inhibits the lysine methyltransferase activity and does not involve the ring nuclease activity nor the host CRISPR immunity. The second involves the ring nuclease activity whose effect is minimized in the presence of type I-A CRISPR targeting.

It is unclear if other RING nuclease proteins act as type III acrs

Although our results clearly demonstrate that SIRV2 gp37 does not have acr function in its biological context, they show it can potentially act as such under the right expression conditions. Thus, we set up to explore if other vRING nucleases in archaea may exhibit acr activity by analyzing their genomic context. Out of 23 vRING nuclease occurrences in crenarchaeal viruses, 7 are associated to genomic regions enriched in anti-defense genes (AFV3-8, SSV13, SSV.M14.15 and SRV), 7 are not associated to anti-defense islands (SIRV1-3, ARV1, AFV9, SIFV1-2) and for 10 it is not possible to determine the functional association of the neighboring genes (turriviruses, bicaudaviruses) due to lack of information about the protein function and genome organization (Figure S6). This suggests that vRING nucleases could be involved in anti-defense roles, including inhibition of type III systems, which are widespread in crenarchaea (Vestergaard, Garrett, and Shah 2014), although it cannot be discarded they are implicated in other defense pathways. However, the frequent presence of vRING nucleases homologs in non-anti-defense genomic contexts together with our results support a role of these proteins beyond inhibition of type III immunity.

As SiL_1451 homologs are restricted to crenarchaea, the interaction between the gp37 and lysine methyltransferase homologs is only relevant for members of this phylum. Importantly, while residues involved in cA_4 cleavage are highly conserved in vRING nucleases, residues involved in binding of SiL_1451 are more variable and conserved only in a few related rudiviruses (Figure S7), hence, protein sequence analysis do not support a widespread conservation of the interaction. On the other hand, the lysine methyltransferase homologs are conserved in the crenarchaeota (67-100% amino acid identity), including near-absolute conservation of the identified gp37-interacting residues (Figure S7). Modelling of complex formation between RING nuclease proteins from crenarchaeal viruses and their cognate host lysine methyltransferase suggests all of the tested protein pairs interact using equivalent

residues for binding (Figure S8); moreover, complex formation was detected between bacterial RING nucleases YddF from *B. subtilis* and *Listeria boonae*, or the DNA-binding protein Sso7d and the clamp protein PCNA, all known substrates of SiL_1451 (Chu et al. 2012) (Figure S8). However, no complex formation was predicted between SiL_1451 and Cren7, another substrate of the crenarchaeal protein methyltransferase. Thus, it is possible the interaction between SiL_1451 and vRING nucleases is a by-product of the broad substrate recognition of the crenarchaeal lysine methyltransferase that happened to be beneficial for viral replication.

DISCUSSION

In this study, we demonstrate RING nuclease gp29 from SIRV1 and its homolog gp37 from SIRV2, previously reported to act as type III anti-CRISPR proteins (Athukoralage et al. 2020), are unable to inhibit type III targeting in their native biological conditions. We show that lack of acr activity is due to the late expression timing of the protein during infection and additionally uncover the interaction between gp37 and SiL_1451, a cellular protein lysine methyltransferase, which results in a mild viral replicative advantage that is independent of the RING nuclease activity of gp37.

While gp29 and gp37 are unable to inhibit type III-B immunity when expressed from their native promoter in the viral genome, plasmid-borne proteins exhibit acr activity and protect a SIRV2 mutant encoding no acrs from type III targeting (Fig. 1D-G). This highlights the importance of immediate inhibition of CRISPR-Cas targeting for acr function and establishment of viral infection. The absence of type III acr activity of gp37 is further supported by the virus competition assays that show cA_4 cleavage is not required for the gp37-conferred replicative advantage and that in wild-type cells gp37 assists viral infection through the inhibition of SiL_1451 (Fig. 4B-C). Furthermore, I-A CRISPR-Cas targeting is required for the gp37-phenotype, as viral competition in a mutant strain lacking I-A targeting uncovers the benefit of gp37 RING nuclease activity (Fig. 4F). Two findings are inferred from this result: i) the first one is that in the native host the presence of CRISPR-Cas immunity determines the mechanism of action of gp37 through SiL_1451 inhibition; ii) second, cA_4 degradation is important in the absence of CRISPR-Cas systems, demonstrating the existence of other pathways of cA_4 generation besides type III systems and a role for this secondary messenger independent of CRISPR immunity. Figure 5 summarizes the above findings and provides a model to explain the role of gp37 alternative activities under different scenarios. The presence of alternative cA_4 synthesis pathways has especial significance given that secondary nucleotide messengers are implicated in signal transduction of developmental, physiological and defense processes in all organisms. In particular, our knowledge about the diversity of secondary

nucleotide messengers involved in defense mechanisms in bacteria (e.g. CBASS, cGAS-STING, Pycsar, type III CRISPR-Cas) has greatly expanded in the last years (Burroughs et al. 2015; Whiteley et al. 2019; Cohen et al. 2019; Lowey et al. 2020; Ye et al. 2020; Millman et al. 2020). Contrastingly, little is known about nucleotide secondary messengers in archaea. A recent study identified the presence of several cyclic and linear nucleotide molecules in *S. acidocaldarius* and *H. volcanii,* although their biological role remains to be determined (Braun et al. 2021). Up to date, the only described role for cA_4 is related to type III CRISPR-Cas immunity and future work shall elucidate alternative functions of cA_4 and other secondary nucleotides in archaea, a very likely scenario given that the role of nucleotide messengers in defense is a conserved feature in the other domains of life. We acknowledge our results do not discard a role as acr for vRING nucleases, albeit they introduce the reasonable presumption that these proteins frequently have alternative roles during viral infection. This inference is supported by the analysis of the genomic neighborhood of vRING nucleases in archaeal viruses, where around half of the gp29 homologs are not encoded in recognizable anti-defense islands, as would be expected for acrs (Figure S6). Moreover, we speculate that the interaction between vRING nucleases and crenarchaeal lysine methyltransferases is the result of the lack of substrate specificity of the latter and whose inhibition is beneficial for viral infection of crenarchaeal hosts. This does not rule out a role for cA_4 degradation, as viral proteins are often multifunctional, a property that is favored when the alternate activities are complementary (Copley 2014) or potentially expand the range of action of the protein to different scenarios (e.g. presence/absence of CRISPR-Cas targeting, Fig. 5).

Equally elusive is the role of the lysine methyltransferase SiL_1451, mediating ample protein methylation in the crenarchaea and which functional significance has not been elucidated (Chu et al. 2016). Our work establishes a link between SiL_1451 and cellular defense and/or stress response. Interestingly, a knockout mutant of the lysine methyltransferase shows differential expression of genes involved in metabolism and genes without functional annotation, plus several genes located in the variable region of the *S. islandicus* strain probably corresponding to integrated viruses (Chu et al. 2016) (Figure S9), supporting a role of protein methylation in stress response. Additionally, differential methylation in response to heat-shock of Cren7, a SiL_1451 substrate, affects the DNA-binding ability of Cren7 potentially impacting chromosomal regulation, suggesting a role of SiL_1451 in mediating epigenetic regulation in response to environmental stress (Ding et al. 2022). The mechanism by which inhibition of SiL_1451 methyltransferase activity aids SIRV2 replication remains to be elucidated. The replicative advantage conferred by gp37 is an example about how mild effects become relevant at the population level and can mediate the selective sweep of a strain in the population.

The use of heterologous systems have allowed the discovery and characterization of multiple novel defense systems in prokaryotes (Doron et al. 2018; L. Gao et al. 2020; L. A. Gao et al. 2022; Vassallo et al. 2022; Uribe et al. 2019; Forsberg et al. 2019; Watters et al. 2018; Marino et al. 2018) and constitute an essential tool when a cultivable isolate of the system under study is not available or it lacks tools for its genetic manipulation. However, heterologous systems may introduce artifacts that lead to erroneous conclusions, among other reasons due to changes in expression level, location or timing with respect to the native system. Therefore, it is of uttermost importance to characterize novel proteins under their native biological conditions whenever possible.

Acknowledgements

We are truly grateful to Jinzhong Lin for providing purified *S. islandicus* Cmr-α Cascade complex and SS1-46 target RNA. Grant XXX.

REFERENCES

Athukoralage, Januka S., Stephen A. McMahon, Changyi Zhang, Sabine Grüschow, Shirley Graham, Mart Krupovic, Rachel J. Whitaker, Tracey M. Gloster, and Malcolm F. White. 2020. "An Anti-CRISPR Viral Ring Nuclease Subverts Type III CRISPR Immunity." *Nature* 577 (7791): 572–75. https://doi.org/10.1038/s41586-019-1909-5.

Bhoobalan-Chitty, Yuvaraj, Thomas Baek Johansen, Nadia Di Cianni, and Xu Peng. 2019. "Inhibition of Type III CRISPR-Cas Immunity by an Archaeal Virus-Encoded Anti-CRISPR Protein." *Cell* 179 (2): 448-458.e11. https://doi.org/10.1016/j.cell.2019.09.003.

Birkenbihl, R. P., K. Neef, D. Prangishvili, and B. Kemper. 2001. "Holliday Junction Resolving Enzymes of Archaeal Viruses SIRV1 and SIRV2." *Journal of Molecular Biology* 309 (5): 1067–76. https://doi.org/10.1006/jmbi.2001.4761.

Braun, Frank, Alejandra Recalde, Heike Bähre, Roland Seifert, and Sonja-Verena Albers. 2021. "Putative Nucleotide-Based Second Messengers in the Archaeal Model Organisms Haloferax Volcanii and Sulfolobus Acidocaldarius." *Frontiers in Microbiology* 12: 779012. https://doi.org/10.3389/fmicb.2021.779012.

Burroughs, A. Maxwell, Dapeng Zhang, Daniel E. Schäffer, Lakshminarayan M. Iyer, and L. Aravind. 2015. "Comparative Genomic Analyses Reveal a Vast, Novel Network of Nucleotide-Centric Systems in Biological Conflicts, Immunity and Signaling." *Nucleic Acids Research* 43 (22): 10633–54. https://doi.org/10.1093/nar/gkv1267.

Chu, Yindi, Zhenfeng Zhang, Qian Wang, Yuanming Luo, and Li Huang. 2012. "Identification and Characterization of a Highly Conserved Crenarchaeal Protein Lysine Methyltransferase with Broad Substrate Specificity." *Journal of Bacteriology* 194 (24): 6917–26. https://doi.org/10.1128/JB.01535-12.

Chu, Yindi, Yanping Zhu, Yuling Chen, Wei Li, Zhenfeng Zhang, Di Liu, Tongkun Wang, et al. 2016. "AKMT Catalyzes Extensive Protein Lysine Methylation in the Hyperthermophilic Archaeon Sulfolobus Islandicus but Is Dispensable for the Growth of the Organism." *Molecular & Cellular Proteomics: MCP* 15 (9): 2908–23. https://doi.org/10.1074/mcp.M115.057778.

Cohen, Daniel, Sarah Melamed, Adi Millman, Gabriela Shulman, Yaara Oppenheimer-Shaanan, Assaf Kacen, Shany Doron, Gil Amitai, and Rotem Sorek. 2019. "Cyclic GMP–AMP Signalling Protects Bacteria against Viral Infection." *Nature* 574 (7780): 691–95. https://doi.org/10.1038/s41586-019-1605-5.

Copley, Shelley D. 2014. “An Evolutionary Perspective on Protein Moonlighting.” *Biochemical Society Transactions* 42 (6): 1684–91. https://doi.org/10.1042/BST20140245.

Deng, Ling, Roger A. Garrett, Shiraz A. Shah, Xu Peng, and Qunxin She. 2013. “A Novel Interference Mechanism by a Type IIIB CRISPR-Cmr Module in Sulfolobus.” *Molecular Microbiology* 87 (5): 1088–99. https://doi.org/10.1111/mmi.12152.

Ding, Niannian, Yuanyuan Chen, Yindi Chu, Cheng Zhong, Li Huang, and Zhenfeng Zhang. 2022. “Lysine Methylation Modulates the Interaction of Archaeal Chromatin Protein Cren7 With DNA.” *Frontiers in Microbiology* 13: 837737. https://doi.org/10.3389/fmicb.2022.837737.

Doron, Shany, Sarah Melamed, Gal Ofir, Azita Leavitt, Anna Lopatina, Mai Keren, Gil Amitai, and Rotem Sorek. 2018. “Systematic Discovery of Antiphage Defense Systems in the Microbial Pangenome.” *Science* 359 (6379): eaar4120. https://doi.org/10.1126/science.aar4120.

Ea, Vorontsov, Rensen E, Prangishvili D, Krupovic M, and Chamot-Rooke J. 2016. “Abundant Lysine Methylation and N-Terminal Acetylation in Sulfolobus Islandicus Revealed by Bottom-Up and Top-Down Proteomics.” *Molecular & Cellular Proteomics : MCP* 15 (11). https://doi.org/10.1074/mcp.M116.058073.

Forsberg, Kevin J, Ishan V Bhatt, Danica T Schmidtke, Kamyab Javanmardi, Kaylee E Dillard, Barry L Stoddard, Ilya J Finkelstein, Brett K Kaiser, and Harmit S Malik. 2019. “Functional Metagenomics-Guided Discovery of Potent Cas9 Inhibitors in the Human Microbiome.” Edited by Wendy S Garrett, Peter Turnbaugh, Peter Turnbaugh, and Joe Bondy-Denomy. *ELife* 8 (September): e46540. https://doi.org/10.7554/eLife.46540.

Foster, Kawanda, Joshua Kalter, Walter Woodside, Rebecca M. Terns, and Michael P. Terns. 2019. “The Ribonuclease Activity of Csm6 Is Required for Anti-Plasmid Immunity by Type III-A CRISPR-Cas Systems.” *RNA Biology* 16 (4): 449–60. https://doi.org/10.1080/15476286.2018.1493334.

Gao, Linyi Alex, Max E. Wilkinson, Jonathan Strecker, Kira S. Makarova, Rhiannon K. Macrae, Eugene V. Koonin, and Feng Zhang. 2022. “Prokaryotic Innate Immunity through Pattern Recognition of Conserved Viral Proteins.” *Science* 377 (6607): eabm4096. https://doi.org/10.1126/science.abm4096.

Gao, Linyi, Han Altae-Tran, Francisca Böhning, Kira S. Makarova, Michael Segel, Jonathan L. Schmid-Burgk, Jeremy Koob, Yuri I. Wolf, Eugene V. Koonin, and Feng Zhang. 2020. “Diverse Enzymatic Activities Mediate Antiviral Immunity in Prokaryotes.” *Science* 369 (6507): 1077–84. https://doi.org/10.1126/science.aba0372.

Guo, Li, Yingang Feng, Zhenfeng Zhang, Hongwei Yao, Yuanming Luo, Jinfeng Wang, and Li Huang. 2008. “Biochemical and Structural Characterization of Cren7, a Novel Chromatin Protein Conserved among Crenarchaea.” *Nucleic Acids Research* 36 (4): 1129–37. https://doi.org/10.1093/nar/gkm1128.

Guo, Yang, Birthe B. Kragelund, Malcolm F. White, and Xu Peng. 2015. “Functional Characterization of a Conserved Archaeal Viral Operon Revealing Single-Stranded DNA Binding, Annealing and Nuclease Activities.” *Journal of Molecular Biology* 427 (12): 2179–91. https://doi.org/10.1016/j.jmb.2015.03.013.

Han, Wenyuan, Yingjun Li, Ling Deng, Mingxia Feng, Wenfang Peng, Søren Hallstrøm, Jing Zhang, et al. 2017. “A Type III-B CRISPR-Cas Effector Complex Mediating Massive Target DNA Destruction.” *Nucleic Acids Research* 45 (4): 1983–93. https://doi.org/10.1093/nar/gkw1274.

Han, Wenyuan, Saifu Pan, Blanca López-Méndez, Guillermo Montoya, and Qunxin She. 2017. “Allosteric Regulation of Csx1, a Type IIIB-Associated CARF Domain Ribonuclease by RNAs Carrying a Tetraadenylate Tail.” *Nucleic Acids Research* 45 (18): 10740–50. https://doi.org/10.1093/nar/gkx726.

Han, Wenyuan, Stefano Stella, Yan Zhang, Tong Guo, Karolina Sulek, Li Peng-Lundgren, Guillermo Montoya, and Qunxin She. 2018. “A Type III-B Cmr Effector Complex Catalyzes the Synthesis of Cyclic Oligoadenylate Second Messengers by

Cooperative Substrate Binding." *Nucleic Acids Research* 46 (19): 10319–30. https://doi.org/10.1093/nar/gky844.

Hatoum-Aslan, Asma, Inbal Maniv, Poulami Samai, and Luciano A. Marraffini. 2014. "Genetic Characterization of Antiplasmid Immunity through a Type III-A CRISPR-Cas System." *Journal of Bacteriology* 196 (2): 310–17. https://doi.org/10.1128/JB.01130-13.

He, Fei, Yuvaraj Bhoobalan-Chitty, Lan B. Van, Anders L. Kjeldsen, Matteo Dedola, Kira S. Makarova, Eugene V. Koonin, Ditlev E. Brodersen, and Xu Peng. 2018. "Anti-CRISPR Proteins Encoded by Archaeal Lytic Viruses Inhibit Subtype I-D Immunity." *Nature Microbiology* 3 (4): 461–69. https://doi.org/10.1038/s41564-018-0120-z.

Jiang, Wenyan, Poulami Samai, and Luciano A. Marraffini. 2016. "Degradation of Phage Transcripts by CRISPR-Associated RNases Enables Type III CRISPR-Cas Immunity." *Cell* 164 (4): 710–21. https://doi.org/10.1016/j.cell.2015.12.053.

Jumper, John, Richard Evans, Alexander Pritzel, Tim Green, Michael Figurnov, Olaf Ronneberger, Kathryn Tunyasuvunakool, et al. 2021. "Highly Accurate Protein Structure Prediction with AlphaFold." *Nature* 596 (7873): 583–89. https://doi.org/10.1038/s41586-021-03819-2.

Kazlauskiene, Migle, Georgij Kostiuk, Česlovas Venclovas, Gintautas Tamulaitis, and Virginijus Siksnys. 2017. "A Cyclic Oligonucleotide Signaling Pathway in Type III CRISPR-Cas Systems." *Science (New York, N.Y.)* 357 (6351): 605–9. https://doi.org/10.1126/science.aao0100.

Kazlauskiene, Migle, Gintautas Tamulaitis, Georgij Kostiuk, Česlovas Venclovas, and Virginijus Siksnys. 2016. "Spatiotemporal Control of Type III-A CRISPR-Cas Immunity: Coupling DNA Degradation with the Target RNA Recognition." *Molecular Cell* 62 (2): 295–306. https://doi.org/10.1016/j.molcel.2016.03.024.

Livak, K. J., and T. D. Schmittgen. 2001. "Analysis of Relative Gene Expression Data Using Real-Time Quantitative PCR and the 2(-Delta Delta C(T)) Method." *Methods (San Diego, Calif.)* 25 (4): 402–8. https://doi.org/10.1006/meth.2001.1262.

Lowey, Brianna, Aaron T. Whiteley, Alexander F. A. Keszei, Benjamin R. Morehouse, Ian T. Mathews, Sadie P. Antine, Victor J. Cabrera, et al. 2020. "CBASS Immunity Uses CARF-Related Effectors to Sense 3'-5'- and 2'-5'-Linked Cyclic Oligonucleotide Signals and Protect Bacteria from Phage Infection." *Cell* 182 (1): 38-49.e17. https://doi.org/10.1016/j.cell.2020.05.019.

Makarova, Kira S., Yuri I. Wolf, Jaime Iranzo, Sergey A. Shmakov, Omer S. Alkhnbashi, Stan J. J. Brouns, Emmanuelle Charpentier, et al. 2020. "Evolutionary Classification of CRISPR–Cas Systems: A Burst of Class 2 and Derived Variants." *Nature Reviews Microbiology* 18 (2): 67–83. https://doi.org/10.1038/s41579-019-0299-x.

Marino, Nicole D., Jenny Y. Zhang, Adair L. Borges, Alexander A. Sousa, Lina M. Leon, Benjamin J. Rauch, Russell T. Walton, et al. 2018. "Discovery of Widespread Type I and Type V CRISPR-Cas Inhibitors." *Science (New York, N.Y.)* 362 (6411): 240–42. https://doi.org/10.1126/science.aau5174.

Märtens, Birgit, Salim Manoharadas, David Hasenöhrl, Lukas Zeichen, and Udo Bläsi. 2014. "Back to Translation: Removal of AIF2 from the 5'-End of MRNAs by Translation Recovery Factor in the Crenarchaeon Sulfolobus Solfataricus." *Nucleic Acids Research* 42 (4): 2505–11. https://doi.org/10.1093/nar/gkt1169.

Martínez-Alvarez, Laura, Ling Deng, and Xu Peng. 2017. "Formation of a Viral Replication Focus in Sulfolobus Cells Infected by the Rudivirus SIRV2." *Journal of Virology*, April. https://doi.org/10.1128/JVI.00486-17.

Mayo-Muñoz, David, Fei He, Jacob Bruun Jørgensen, Poul Kári Madsen, Yuvaraj Bhoobalan-Chitty, and Xu Peng. 2018. "Anti-CRISPR-Based and CRISPR-Based Genome Editing of Sulfolobus Islandicus Rod-Shaped Virus 2." *Viruses* 10 (12): E695. https://doi.org/10.3390/v10120695.

Millman, Adi, Sarah Melamed, Gil Amitai, and Rotem Sorek. 2020. "Diversity and Classification of Cyclic-Oligonucleotide-Based Anti-Phage Signalling Systems." *Nature Microbiology* 5 (12): 1608–15. https://doi.org/10.1038/s41564-020-0777-y.

Niewoehner, Ole, Carmela Garcia-Doval, Jakob T. Rostøl, Christian Berk, Frank Schwede, Laurent Bigler, Jonathan Hall, Luciano A. Marraffini, and Martin Jinek. 2017. “Type III CRISPR-Cas Systems Produce Cyclic Oligoadenylate Second Messengers.” *Nature* 548 (7669): 543–48. https://doi.org/10.1038/nature23467.

Peng, Wenfang, Mingxia Feng, Xu Feng, Yun Xiang Liang, and Qunxin She. 2015. “An Archaeal CRISPR Type III-B System Exhibiting Distinctive RNA Targeting Features and Mediating Dual RNA and DNA Interference.” *Nucleic Acids Research* 43 (1): 406–17. https://doi.org/10.1093/nar/gku1302.

Quax, Tessa E. F., Marleen Voet, Odile Sismeiro, Marie-Agnes Dillies, Bernd Jagla, Jean-Yves Coppée, Guennadi Sezonov, et al. 2013. “Massive Activation of Archaeal Defense Genes during Viral Infection.” *Journal of Virology* 87 (15): 8419–28. https://doi.org/10.1128/JVI.01020-13.

Rostøl, Jakob T., and Luciano A. Marraffini. 2019. “Non-Specific Degradation of Transcripts Promotes Plasmid Clearance during Type III-A CRISPR–Cas Immunity.” *Nature Microbiology* 4 (4): 656–62. https://doi.org/10.1038/s41564-018-0353-x.

Samai, Poulami, Nora Pyenson, Wenyan Jiang, Gregory W. Goldberg, Asma Hatoum-Aslan, and Luciano A. Marraffini. 2015. “Co-Transcriptional DNA and RNA Cleavage during Type III CRISPR-Cas Immunity.” *Cell* 161 (5): 1164–74. https://doi.org/10.1016/j.cell.2015.04.027.

Schneider, Caroline A., Wayne S. Rasband, and Kevin W. Eliceiri. 2012. “NIH Image to ImageJ: 25 Years of Image Analysis.” *Nature Methods* 9 (7): 671–75. https://doi.org/10.1038/nmeth.2089.

Uribe, Ruben V., Eric van der Helm, Maria-Anna Misiakou, Sang-Woo Lee, Stefan Kol, and Morten O. A. Sommer. 2019. “Discovery and Characterization of Cas9 Inhibitors Disseminated across Seven Bacterial Phyla.” *Cell Host & Microbe* 25 (2): 233-241.e5. https://doi.org/10.1016/j.chom.2019.01.003.

Vassallo, Christopher N., Christopher R. Doering, Megan L. Littlehale, Gabriella I. C. Teodoro, and Michael T. Laub. 2022. “A Functional Selection Reveals Previously Undetected Anti-Phage Defence Systems in the E. Coli Pangenome.” *Nature Microbiology* 7 (10): 1568–79. https://doi.org/10.1038/s41564-022-01219-4.

Vestergaard, Gisle, Roger A. Garrett, and Shiraz A. Shah. 2014. “CRISPR Adaptive Immune Systems of Archaea.” *RNA Biology* 11 (2): 156–67. https://doi.org/10.4161/rna.27990.

Watters, Kyle E., Christof Fellmann, Hua B. Bai, Shawn M. Ren, and Jennifer A. Doudna. 2018. “Systematic Discovery of Natural CRISPR-Cas12a Inhibitors.” *Science (New York, N.Y.)* 362 (6411): 236–39. https://doi.org/10.1126/science.aau5138.

Whiteley, Aaron T., James B. Eaglesham, Carina C. de Oliveira Mann, Benjamin R. Morehouse, Brianna Lowey, Eric A. Nieminen, Olga Danilchanka, et al. 2019. “Bacterial CGAS-like Enzymes Synthesize Diverse Nucleotide Signals.” *Nature* 567 (7747): 194–99. https://doi.org/10.1038/s41586-019-0953-5.

Ye, Qiaozhen, Rebecca K. Lau, Ian T. Mathews, Erica A. Birkholz, Jeramie D. Watrous, Camillia S. Azimi, Joe Pogliano, Mohit Jain, and Kevin D. Corbett. 2020. “HORMA Domain Proteins and a Trip13-like ATPase Regulate Bacterial CGAS-like Enzymes to Mediate Bacteriophage Immunity.” *Molecular Cell* 77 (4): 709-722.e7. https://doi.org/10.1016/j.molcel.2019.12.009.

Zheng, Lei, Ulrich Baumann, and Jean-Louis Reymond. 2004. “An Efficient One-Step Site-Directed and Site-Saturation Mutagenesis Protocol.” *Nucleic Acids Research* 32 (14): e115. https://doi.org/10.1093/nar/gnh110.

Zillig, Wolfram, Arnulf Kletzin, Christa Schleper, Ingelore Holz, Davorin Janekovic, Johannes Hain, Martin Lanzendörfer, and Jakob K. Kristjansson. 1993. “Screening for Sulfolobales, Their Plasmids and Their Viruses in Icelandic Solfataras.” *Systematic and Applied Microbiology* 16 (4): 609–28. https://doi.org/10.1016/S0723-2020(11)80333-4.

FIGURES

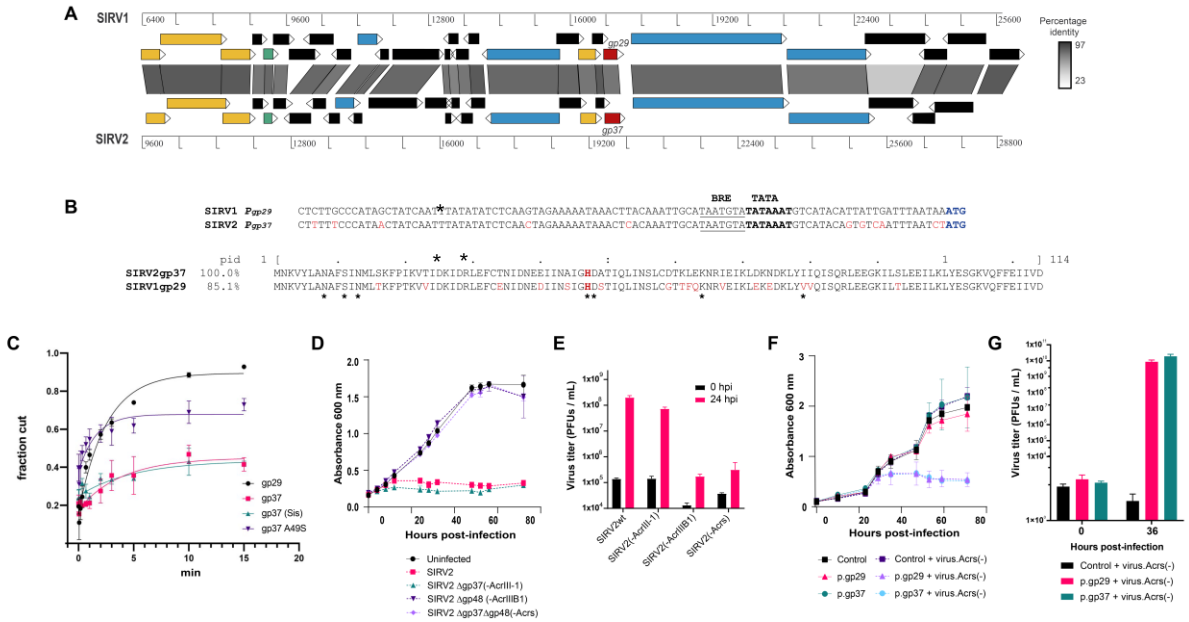

Fig. 1. The AcrIII-1 homolog gp37 does not inhibit subtype III-B CRISPR immunity in SIRV2-infected cells. A) Comparison of the AcrIII1 genomic neighborhood in SIRV1 and SIRV2. AcrIII1 homologs are encoded in a four-gene operon together with highly conserved rudiviral genes. Open-reading frames are colored according to their functional category: yellow – DNA metabolism; green – transcription; blue – virion proteins; red – AcrIII-1 homologs. **B)** Alignment of the promoter region (top) and amino acid sequence (bottom) of AcrIII-1 homologs in SIRV1 and SIRV2. pid – percentage identity. Nucleotides that differ in P_{gp29} with respect to P_{gp37} are indicated in red. The start codon is highlighted in blue. The core promoter elements TATA-box and BRE are shown in bold and underlined, respectively. **C)** Kinetic rate of cA_4 degradation of the rudiviral AcrIII-1 proteins. Average and s.d. values three biological replicates. Recombinant proteins were expressed and purified from *E. coli*, except gp37 (Sis), expressed and purified from *S. islandicus* LAL14/1. **D-E)** The AcrIII-1 homologs SIRV2 gp37 or SIRV1 gp29 cannot inhibit native targeting by III-B immunity. D) CRISPR III-B (+) cultures were infected with the indicated viruses with an MOI of 0.01 and cell growth was monitored by measuring optical density at 600 nm. E) Determination of the extracellular virus titer in the cultures from panel D. Average and s.d. values from three biological replicates. **F-G)** Plasmid-borne expression of AcrIII-1 homologs exhibits type III-B anti-CRISPR activity. F) Growth curves of CRISPR (+) strains carrying plasmid-borne AcrIII-1 homologs with and without infection by SIRV2 Δacrs. G) Virus titer at 0 and 36 hours post-infection in the supernatant of cultures from panel F. Results from three biological replicates, bars indicate the s.d.

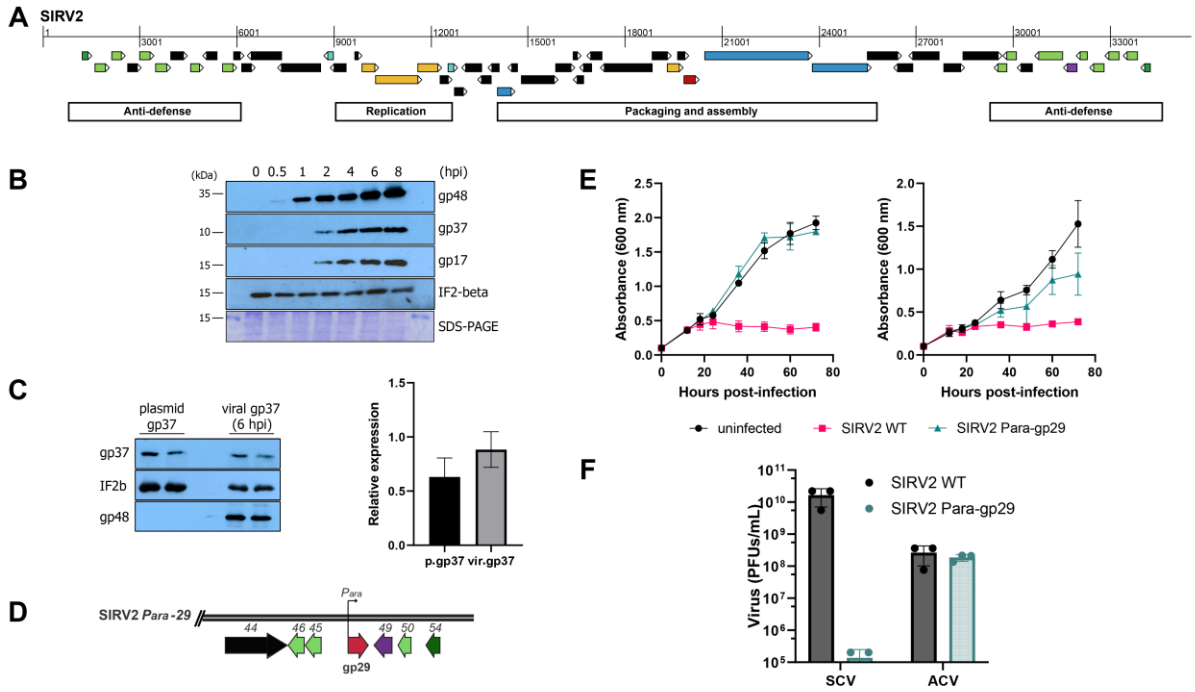

Figure 2. SIRV2 gp37 middle/late expression pattern curbs its ability to exert III-B anti-CRISPR activity. A) Functional partitioning of the genome of SIRV2 indicating the regions enriched in genes involved in anti-defense, replication and virion assembly and maturation. The color of the open-reading frames corresponds to: dark green – Aca8 homologs; light green – AcrID1 and AcrIIIB1 homologs; turquoise – transcriptional regulators; yellow – genes involved in DNA replication and metabolism; blue – structural genes; red – AcrIII-1; purple – cell lysis. **B)** Expression kinetics of early (gp48) and middle/late (gp17 and gp37) viral proteins in SIRV2-infected cells determined by western blot. A representative experiment from three biological replicates is shown. **C)** Expression level of plasmid-borne and virally-encoded gp37. Left: representative western blot of plasmidic gp37 and SIRV2-infected lysates at 6 hours post-infection (hpi). Right: average relative levels of gp37 normalized to IF2 expression from three independent biological replicates and bars corresponding to the s.d. **D-F)** Early expression of AcrIII-1 exhibits acr-activity during SIRV2 infection. D) Schematic representation of the genome of the recombinant virus SIRV2 *Paragp29*, where *acrIIIB1* (*gp48*) is substituted by the *acrIII-1* homolog in SIRV1 under the control of the inducible arabinose promoter (*Para*gp29). Coloring of open-reading frames is the same as described in panel A. E) Growth curves of CRISPR III-B (+) cultures infected with wild-type SIRV2 (wt) or SIRV2 *Para*gp29 (*Para*gp29) at an MOI of 0.1 before (left) and after (right) induction of gp29 expression with arabinose (final concentration 0.2%). F) Average and s.d. values of extracellular virus titers from infected cultures at 36 hpi. Data from two biological replicates.

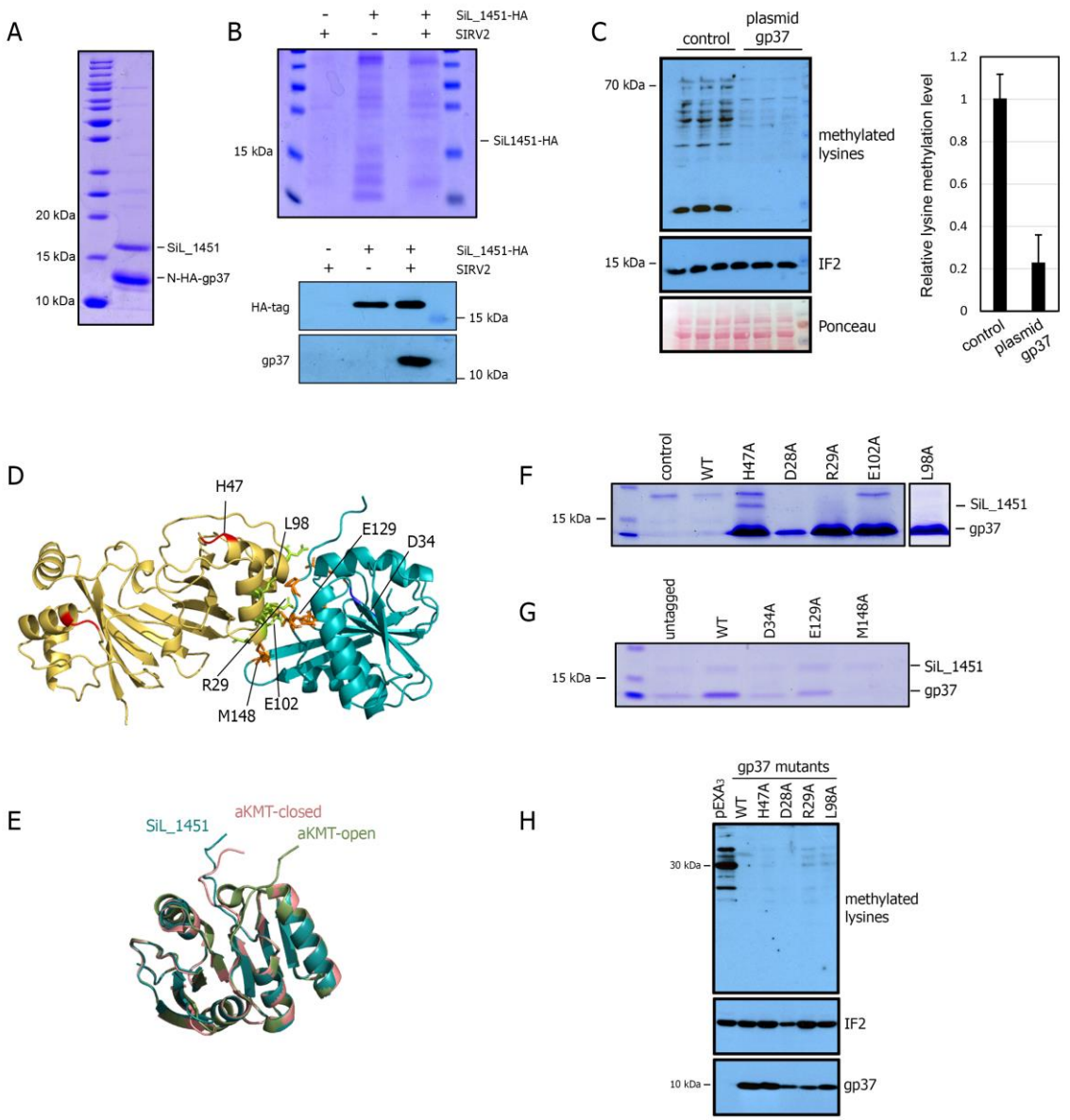

Figure 3. SIRV2 gp37 binds and inhibits the cellular protein lysine methyltransferase SiL_1451. A-B) Co-purification of HA-gp37 and SiL_1451. Pull-down assay using a virally encoded gp37 bearing an N-terminal HA-tag **(A)** Pull-down assay with plasmid-borne C-terminally HA-tagged SiL_1451 with or without infection with SIRV2 **(B, top)** and western blot using anti-HA and anti-gp37 antibodies **(B, bottom)**. **C)** Plasmid-expressed gp37 inhibits protein lysine-methylation levels. Left: representative western blot of cellular lysates (*n*=3) using polyclonal antibodies to mono- and di-methyl lysines or translation initiation factor 2 beta (IF2) as a loading control. Right: average relative lysine methylation levels with s.d. from three biological replicates. **D)** Model of the complex between a gp37 dimer and SiL_1451. Red: residues important for ring nuclease activity. Blue: SiL_1451 catalytic residues. Green and orange: residues involved in the interaction between gp37 and SiL_1451, respectively. **E)** Comparison of the structures of SiL_1451-SAH (aKMT-open,green),

SiL_1451-SAM (aKMT-closed, pink) and gp37-bound SiL_1451 (blue). **F)** Pull-down assay of plasmid-expressed C-terminally His-tagged gp37 mutants. **G)** Pull-down of plasmid-expressed untagged gp37 and N-terminally His-tagged SiL_1451 variants. **H)** Representative western blot (*n* = 3) of the lysine methylation levels in cellular lysates from panel G.

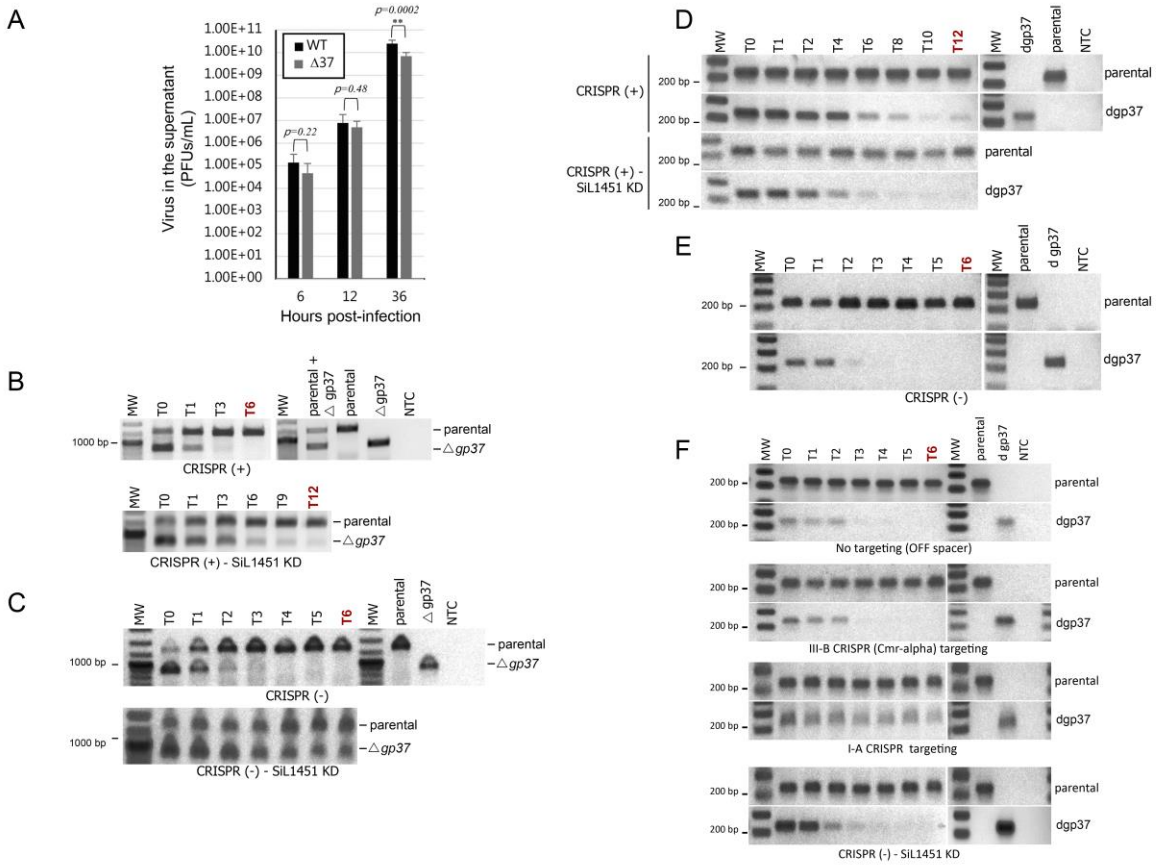

Figure 4. The two activities of SIRV2 gp37 confer viral replicative advantage under different scenarios. **A)** Production of virus progeny (PFUs/mL) in a CRISPR (-) host infected with the parental SIRV2 or a Δgp37 deletion mutant. Data corresponds to the average and s.d. of eight biological replicates. **B-E)** Competition assay between parental SIRV2 (gp37 wt) and a virus lacking gp37 (Δgp37) or encoding a variant of gp37 without ring nuclease activity (d gp37). Presence of viruses in the supernatant was monitored by qualitative PCR using primers specific for each viral strain. Cultures of CRISPR (+) (B-C), CRISPR (+) - *SiL_1451* knockdown (B-C) or CRISPR (-) (D-E) hosts were infected with an equimolar mixture of the indicated viruses at an MOI of approximately 0.0001. **F)** Same as B-E but host cultures correspond to a strain carrying a spacer with no match on SIRV2 (first panel, off spacer), CRISPR (+) III-B cells (second panel), a CRISPR (+) I-A carrying a spacer able to elicit I-A immunity but unable to activate III-B immunity as the crRNA is not complementary to the target gene transcript (third panel), or a CRISPR (-) - *SiL_1451* knockdown host (bottom panel).

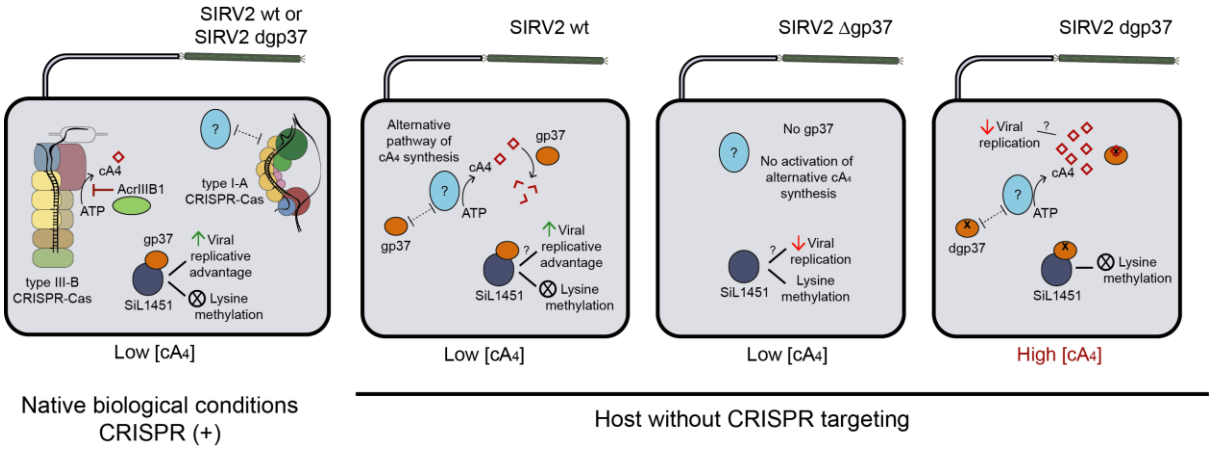

Figure 5. Model of the effect of multifunctional gp37 during SIRV2 infection under diverse scenarios. *First panel*: During SIRV2-infection of the native host *S. islandicus* LAL14/1 intracellular cA_4 levels are kept low through the inhibition by viral AcrIIIB1 of the type III-B CRISPR-Cas and by the effect of the activation of type I-A CRISPR-Cas over alternative sources of cA_4 production. Thus, the RING nuclease activity of gp37 is dispensable in this scenario. Interaction between gp37 and lysine methyltransferase SiL_1451 results in the inhibition of the latter, abrogation of cellular protein lysine methylation and a positive effect on viral replication through a yet unknown mechanism. Second to fourth panels correspond to infection with the indicated SIRV2 strains of a host without CRISPR-Cas mediated targeting of the virus. *Second panel*: Infection by wild-type (wt) SIRV2. Lack of I-A CRISPR-Cas targeting and presence of gp37 activates an alternate cA_4 synthesis pathway unrelated to type III-B CRISPR-Cas. This cA_4 is rapidly degraded by the RING nuclease activity of gp37, keeping cA_4 intracellular levels low. Similar to the first panel, inhibition of SiL_1451 by gp37 is beneficial for viral replication. *Third panel*: Infection by SIRV2 Δgp37 mutant lacking gp37. Absence of gp37 fails to trigger the alternate cA_4 synthesis pathway, thus intracellular concentration of this nucleotide is low and RING nuclease activity is not necessary. Nevertheless, active SiL_1451 has a mild negative impact on SIRV2 replication through an unidentified mechanism. *Fourth panel*: Infection by SIRV2 d gp37 encoding a gp37 with abrogated RING nuclease activity. Presence of gp37 activates alternate cA_4 production, which negatively affects viral replication, overcoming the positive impact of the gp37-mediated inhibition of SiL_1451. Dotted lines represent a yet unidentified direct or indirect interaction between two protein complexes. Interrogation signs indicate unknown mechanism of action.

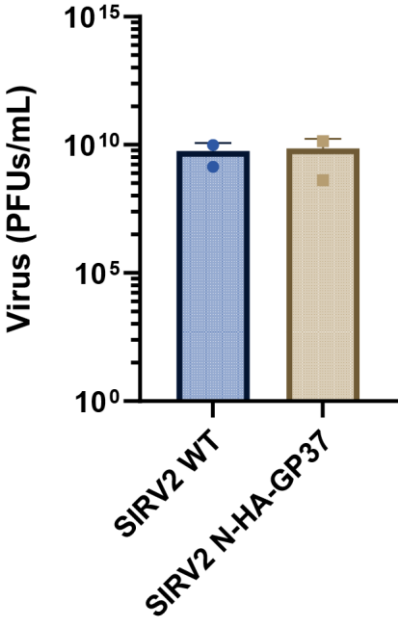

Figure S1. Virus mutant SIRV2 N-HA-gp37 with an N-terminally hemagglutinin tagged gp37 is similarly infective as the parental virus. CRISPR (-) cultures were infected with the corresponding virus at an MOI of 0.01 and virus in the supernatant was determined after 36 h.

MS analysis 1: NHA-gp37

Id#	Id	Protein name	Coverage	MW	Score
1.1	THSA_SACSH	Thermosome subunit alpha OS=Saccharolobus shibatae OX=2286 GN=thsA PE=1 SV=1	46.6 %	59723	1485
1.2	KMT_SULIR	Protein-lysine N-methyltransferase OS=Sulfolobus islandicus (strain REY15A) OX=930945 GN=SiRe_1449 PE=1 SV=1	85.7 %	18200	1267

1.2 Protein identification information

Protein-lysine N-methyltransferase OS=Sulfolobus islandicus (strain REY15A) OX=930945 GN=SiRe_1449 PE=1 SV=1

Protein ID: KMT_SULIR	MW: 18200	pI: 6.11
Mascot score: 1267	Seq. Coverage: 85.7 %	Unique peptides: 22
Uniprot link	***Conserved Domain link***	***Blast link***

Peptide map:

```
  1 MSYVPHVPYV PTPEKVVRRM LEIAKVSQDD IVYDLGCGDG RIIITAAKDF NVKKAVGVEI
 61 NDERIREALA NIEKNGVTGR ASIVKGNFFE VDISEATVVT MFLLTNVNEM LKPKLEKELK
121 PGTRVVSHEF EIRGWNPKEV IKVEDGNMNH TVYLYVIGEH K
```

Variable modifications:

Oxidation:

M: 20;148

Id#	Id	Protein name	Coverage	MW	Score
1.1	N-HA-gp37	nan	44.7 %	14423	376

1.1 Protein identification information

nan

Protein ID: N-HA-gp37	MW: 14423	pI: 4.82
Mascot score: 376	Seq. Coverage: 44.7 %	Unique peptides: 7
Uniprot link	***Conserved Domain link***	***Blast link***

Peptide map:

```
  1 MYPYDVPDYA NKVYLANAFS INMLSKFPIK VTIDKIDRLE FCTNIDNEEI INAIGHDATI
 61 QLINSLCDTK LEKNRIEIKL DKNDKLYIIQ ISQRLEEGKI LSLEEILKLY ESGKVQFFEI
121 IVD
```

Variable modifications:

Oxidation:

M: 23

896

Figure S2. Nanoscale liquid chromatography coupled to mass spectrometry results of protein eluate in Fig. 3A. The analysis identifies the 18 kDa band as the lysine methyltransferase SiRe_1449 corresponding to SiL_1451 in *S. islandicus* LAL14/1 and the 14.4 kDa band as SIRV2 gp37.

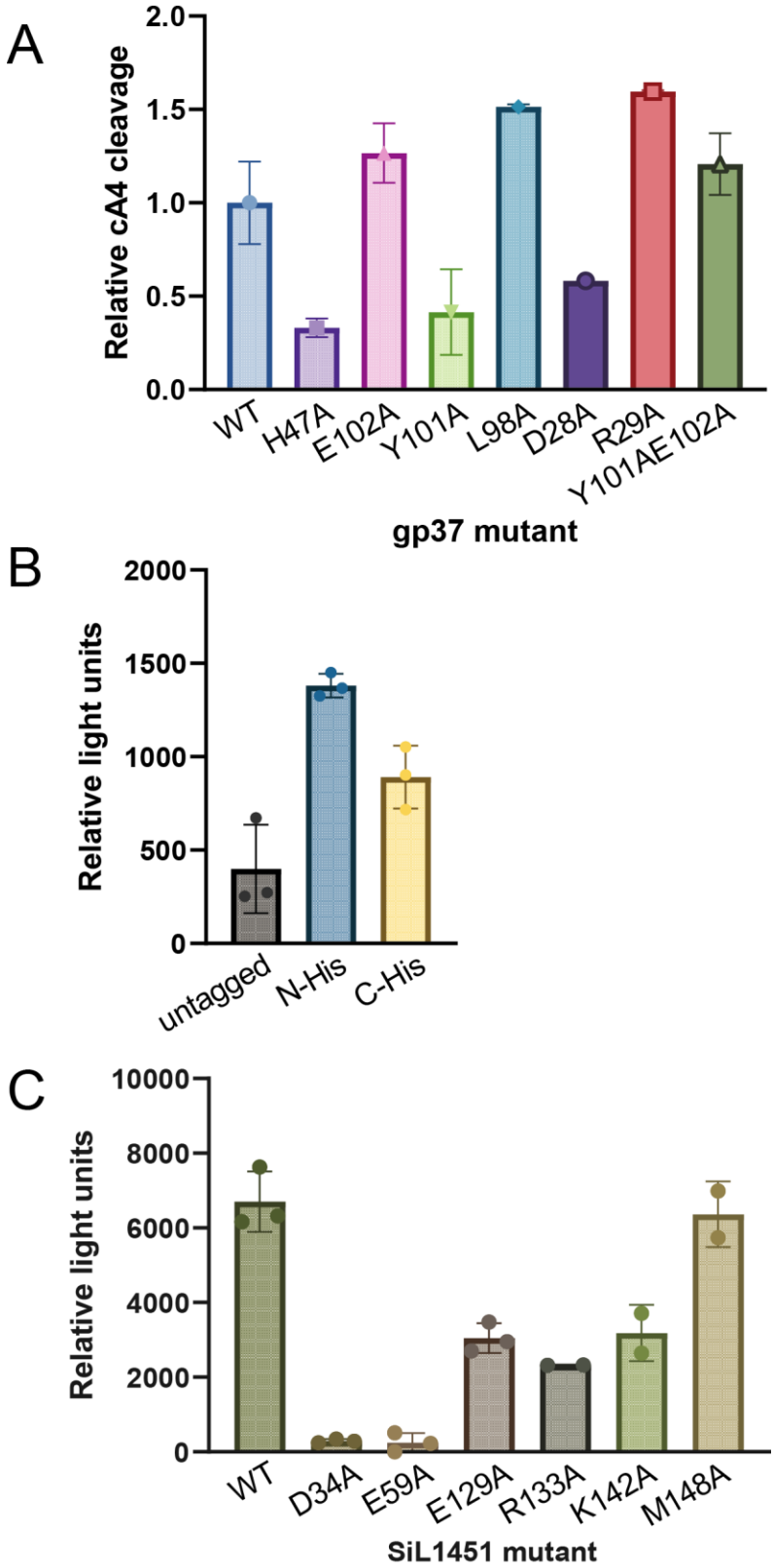

Figure S3. Catalytic activity of gp37 and SiL_1451 alanine mutants of putative gp37-SiL_1451 interaction residues. A) cA_4 cleavage activity of gp37 mutants relative to the wild-type (WT) protein. Mutant H47A is a catalytically defective RING nuclease, as previously described by Athukoralage et al. (2019). Mutants Y101A and D28A show abrogated cA_4

cleavage capacity and were not used in downstream assays. **B)** Effect of His-tag placement on the methyltransferase activity of SiL_1451. Methyltransferase activity was measured with the MTase-Glo™ assay using Cren7 as the substrate, as described in methods. The untagged SiL_1451 protein was obtained from enterokinase treatment of the N-terminally His-tagged recombinant protein. The N-terminally tagged SiL_1451 (N-His) was used for mutant construction as it displays the highest methyltransferase activity. **C)** Methyltransferase activity of SiL_1451 mutants. Mutants D28A and E59A are unable to bind the cofactor SAM as reported previously (Chu et al. 2010) and thus display no methyltransferase activity. All mutants tested, with the exception of M148A, have reduced methyltransferase activity. The data correspond to the average of two or three biological replicates. Bars correspond to the standard deviation.

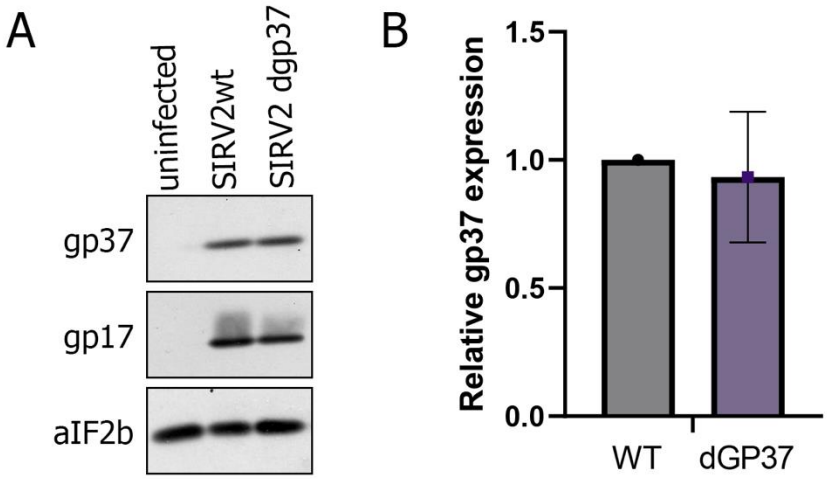

Figure S4. Expression level of gp37 in the virus mutant SIRV2 dgp37 is comparable to the expression in the parental strain. CRISPR (-) cultures were infected with an MOI of 3 with the parental strain SIRV2 (wt) or mutant SIRV2 d gp37 encoding a catalytically dead gp37 (H47A mutant). Samples were collected at 3 hpi and analyzed by western blot. Data was normalized using aIF2β as loading control and dgp37 protein level is reported relative to wild-type gp37 expression. **A)** Representative western blot of infected cellular lysates (*n*=3). **B)** Relative average d gp37 expression with s.d. from three biological replicates.

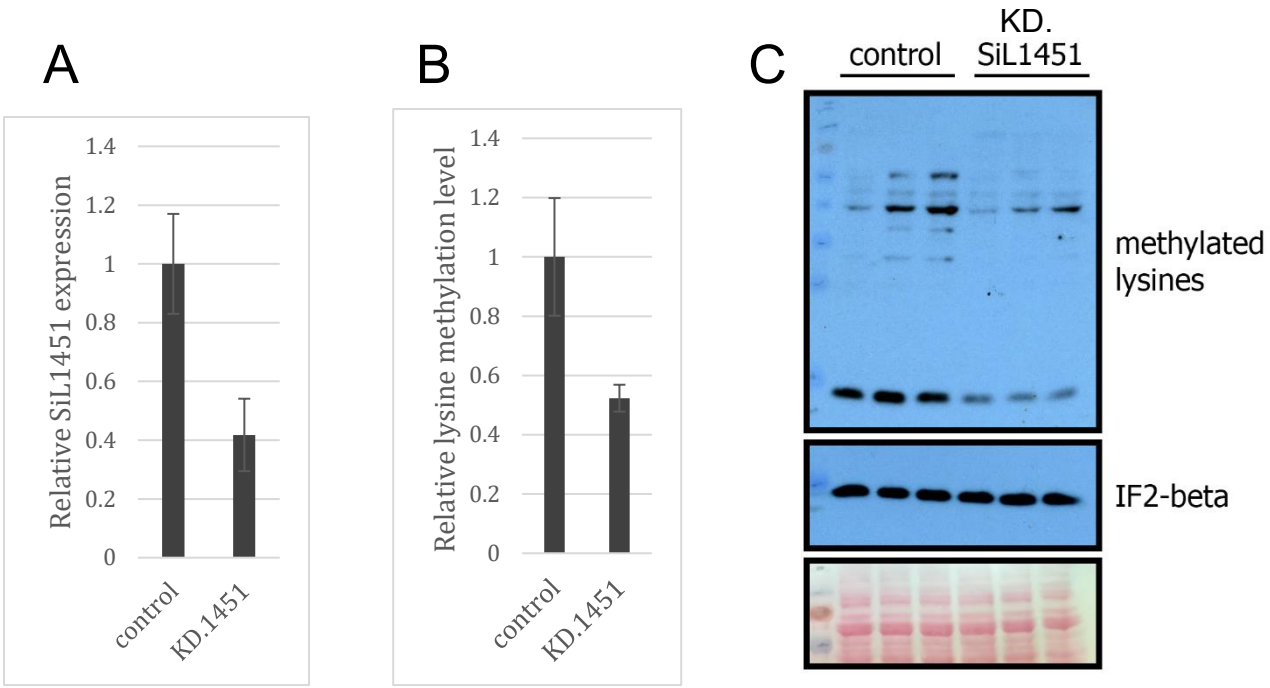

Figure S5. CRISPR-based silencing of SiL_1451 expression. A) Transcription level of *siL_1451* determined by RT-qPCR in samples of control culture (harboring an empty plasmid) and SiL_1451 knock-down strain (KD.1451) at OD600 = 0.2. Data represent the average and s.d. *siL_1451* mRNA of three biological replicates. **B)** Relative lysine methylation level of cultures in panel A as determined by western blot. Data correspond to average lysine methylation and s.d. of three biological replicates. **C)** Representative western blot of cellular lysates in panel B. IF2β was used as loading control.

VIRUS	vRING	Acr IIIB1	AcrID	ANTI-DEFENSE ISLAND	COMMENTS ON GENE NEIGHBORHOOD
SIRV1				N	with Holliday junction resolvase
SIRV2				N	with Holliday junction resolvase
SIRV3				N	with Holliday junction resolvase
SIRV4					
SIRV5					
SIRV6					
SIRV7					
SIRV8					
SIRV9					
SIRV10					
SIRV11					
ARV1				N	With single-strand DNA binding protein
ARV2					Near by a TFBII homolog
SRV				Y	Genome end and next to Aca8
SSRV1					
AFV1					Cluster of hypothetical proteins, opposite end to AcrID
AFV2					
AFV3				Y	Close to AcrIIIB1
AFV6				Y	Close to AcrIIIB1
AFV7				Y	Close to AcrIIIB1
AFV8				Y	Close to AcrIIIB1
AFV9				N	Cluster of transcriptional regulators
SIFV				N	Cluster of transcriptional regulators
SIFV2				N	Cluster of transcriptional regulators
SMF1					
ATV					
ATV2					
SMV4					
SSV.M14.25				Y	Transcript T5, variable region
SSV13				Y	Transcript T5, variable region
STIV					Cluster of hypothetical proteins
STIV2					Cluster of hypothetical proteins
SMV2					
SSV3					
SSV6					
SSV2					

Figure S6. Genome neighborhood analysis of vRING nuclease homologs in archaeal viruses. Viruses with homologs of vRING nuclease proteins, AcrIIIB-1 or AcrID were retrieved and the location of vRING nuclease homologs was analyzed. Homologs of vRING nucleases in the vicinity of an Acr or Aca protein and in a cluster of small hypothetical genes coded in the same strand were annotated as encoded in an anti-defense island.

A

```
SIRV2gp37_NP_666571.1   ------------MNKVYLANAFSINMLS------KFPIKVTIDKIDRLEFCTNI----DNEEIINA-IGHDATIQLINSLCDTKLEKNRIEIKLDKNDKLYIIQISQRLEE--------------------------GKIL--SLEEILKLYESGKVQFFE----IIVD----------------------------------
SIRV1gp29_NP_666617.1   ------------MNKVYLANAFSINMLT------KFPTKVVIDKIDRLEFCENI----DNEDIINS-IGHDSTIQLINSLCGTTFQKNRVEIKLEKEDKLYVVQISQRLEE--------------------------GKIL--TLEEILKLYESGKVQFFE----IIVD----------------------------------
SIRV3_YP_009272980.1    ------------MNKNYLANAFSINMLS------KFPIKVTIDKIDRLEFCTNI----DNEEIINA-IGHDSTVQLINSLCDTKFEKNRIEIKLDKRDKLYIVQISQRLEE--------------------------GKIL--TLEEILKLYETGKVQFFE----IIVD----------------------------------
SSRV1_QJF12309.1        -------------MVLYLLNSLIVPFE------GQEAEFQIKKINFKEARDIVN---NAGNIVSA-IGHSATANILSNLLGIPVQTSRIAIYFKPGDNAIAFVLKRRLEE--------------------------GQVI-QTEEELNKIG-------YD----LYYILRIR--------------------------------
AFV9_YP_001798543.1     --------------MLYVLNSATLPLKP------GKEYMIRARELTIEEAKELL----STEPYVSA-VGHEATAVALSNIFGVTIPYNRTQIFLDKGDKLLSIILKKRLEE--------------------------GKVI-KTVEELQQVG-------YS----IWLFEVEPDGQKELGNPGIV--------------------
SSV.M.16.25_AZG03274.1  --------------MIYLTNGFSPSMLS------VDGAIIIHKKISVTEFCEGVK---DERNIINA-IGHKSTAEIVNMLCKTNYQMNRISIKLKPGDVAYVVTLTVRLEE--------------------------GTIL--GSGDIAAFYEQGKLAFFKYEIRAWNNECEKALNELVENAGRLDERGYDTLSMQIANCWLVR
SSV13_AZG03070.1        --------------MIYLTNGFSPSMLS------VDGAIIIHKKISVTEFCEGVK---DERNIINA-IGHKSTAEIVNMLCKTNYQMNRISIKLKPGDVAYVVTLTVRLEE--------------------------GTIL--GSGDIAAFYEQGKLAFFKYEIRAWNNECEKALNELVENAGRLDERGYDTLSMQIANCWLVR
ARV2_YP_009230246.1     -------------MVLYLLNSLIIPIQ------DNEAEFKIKRISISEARDIVD---NAQQVISA-IGHSATASVMSALLGMPVETNRIPIYFKVGDSAIAIVLRQRLPE--------------------------GHVI-QSEDELQKIG-------YD----LYYIERVR--------------------------------
SMV4_YP_009218525.1     -------------MTVYLANAFSPSMLN------KLPSAVEFQRVDQKEFCEAI-----HHGVSNA-IGHKGTIEFVNTLCNTNLQTNRVEIKAGINDVIYIIVLGFRLEE--------------------------GKVL--SAGEVQKAYDEGKVLLLK----AIIGK----------------------------------
SRV_YP_009094261.1      ------------MVRVILVNSFSINMIT------DDKVNIRFVKINFDKAREIIELAKKKNIKVESYIGHESTAQLLTRLLNYNIVTNRTEYKLQPTDVLLIFSLSKRLSKPEDIANINESEFNVFIAVVVDLWIAPGTVILSTDSEITNIFPE-LIDLVS----EWMMAG--------------------------------
SMF1_YP_007678016.1     MVTQTQTQKSEGEGVIFLANAFAPSMLL------CTKSTVVFERVSAEQARRLI----AGKKTVSY-VGHDSTANAMAVLLGIEVPVNRSALKLTSGE-LIVFSLNQRLPE--------------------------GKVL-KTMQELESVG-------YT----IYHVIVRCE--------------------------------
STIV2B16_YP_003591092.1 ------------MGKTYLVNAFSLNMIK------NFPANVVIDKIDKDEFCTTID--TEEEYLVNA-VGHDSTIALINTLCGTKLQKNRVEIKLDKGDRAIVIMITQRLEE--------------------------GKVL--NHEEITKMYEEGKIGFYE----VWIK----------------------------------
AFV8gp13_YP_001604294.1 --------------MLYILNSAILPLKP------GEEYLIKAKEINIEQAKKLV----QNEKFTSA-IGHDATAKLLSNILEVNVTMNRIAIRVSHGDKILAFLLKQRLPE--------------------------GTVI-KSVEELEKIG-------YE----LWLFEIQ--------------------------------
AFV7gp11_YP_001604235.1 --------------MLYILNAQILPLKP------GEEYTVKARQISIEEARELV----KKENFTSA-IGHQATAELLTNVLGVNVPVNRIAIRATHGDKIIAFSLKQRLPE--------------------------GVVI-KTTEELEKIG-------YE----LWLFEIQ--------------------------------
AFV6gp16_YP_001604174.1 --------------MLYLLNSAILPLKE------GEEYIVKAKEITIQEARELL----HKENFVSA-VGHQATAELLSNVLGVNIPVNRIAIKASHGDKILAFSLKQRLPE--------------------------GVVI-KTTEELEKIG-------YE----LWLFEIQ--------------------------------
AFV3_YP_001604358.1     --------------MLYILNSAILPLKP------GEEYTVKAKEITIQEAKELV----TKEQFTSA-IGHQATAELLSSILGVNVPMNRVQIKVTHGDRILAFMLKQRLPE--------------------------GVVV-KTTEELEKIG-------YE----LWLFEIQ--------------------------------
ARV1_YP_001542630.1     --------------MLYILNAQITPFE------GAQATFVERRIDVNEAKKIV----NSQPFVSA-VGHAATAQLLSKLLDASIPTNRTQVFLKPGDMALAIVLKSRIPE--------------------------GVVL--DEQAIRNIG-------FE----IVVIERVS--------------------------------
ATVgp06_YP_319837.1     --------MGVWSVVLYLLNTLIVPFR------DERAKFEIERVSAEEAKKIIQ--MHNSQFVSA-IGHSASANALSLLLGVAVPVNRTEVFFNVGDEAIAMALKKRLAE--------------------------GQVL-RTVQELEAVG-------FD----LYYIKRVQ--------------------------------
STIV1B116_YP_025003.1   ------------MGKVFLTNAFSINMLK------EFPTTITIDKLDEEDFCLKLELRLEDGTLINA-IGHDSTINLVNTLCGTQLQKNRVEVKMNEGDEALIIMISQRLEE--------------------------GKVL--SDKEIKDMYRQGKISFYE----VW----------------------------------
AFV1ORF116_YP_003762.1  --------------MGSYLLNGFSPAMLA------SGHSVVFFNQIPDVMLCGAL----TSDELVNA-IGHKSTINLINRICQTNLKENRIQVMLQDGDEAFIVVVTERLEE--------------------------GKVL--SDEEITKMFEDGKIKIYY----ARVHSVV--------------------------------
SIFV_NP_445691.1        --------------MLYILNSATLPLKP------GKEYVIHAKELTIEEAKELL----ENERFISA-VGHEATAKMLTNIFDVEIPMNRIQIFLDDGDKLLSIILKTRLEE--------------------------GKVI-KTVEELEQIG-------YN----IWLFEVVTYEHNVKYE--------------------
SIFV2_AOS58378.1        --------------MLYILNSATLPLKP------GKEYVIHAKELTIEEAKELL----ENERFISA-VGHEATAKMLTNIFGVEISMNRIQIFLDDGDKLLSIILKTRLEE--------------------------GKVI-KTVEELEQIG-------YN----IWLFEVVTYVHNAKYE--------------------
ATV.vl_AON96486.1       --------MGVWSVVLYLLNTLIVPFR------DERAKFEIERVSAEEAKKIIQ--MHNSQFVSA-IGHSASANALSLLLGVAVPVNRTEVFFNVGDEAIAMALKKRLAE--------------------------GQVL-RTVQELEAVG-------FD----LYYIKRIQ--------------------------------
ATV2_AON96424.1         --------MGVWYVVLYLLNTLIVPFRDLIVPFRDERAKFEIERVSVEEAKEMTP--------------------------------------------------------------------------SKVI-------SFF-------YR----LFFSDLK--------------------------------
yddf_B.subtilis         -------------MEIAFLNSLVV----------TSPGFYKAEKITLDEVKQWLK--HYDGRYKSF-IGHKSTAQFLQKLLGIRIEQNRKTFRHMKYQKAICFSLYERYPE--------------------------NVLL--TQRDLEKAR-------YQ----FYLLTRLD--------------------------------
```

B

```
AAK40871.1 SSO P2                ---MSYVPHVPYVPTPEKVVRRMLEIAKASQDDIVYDLGCGDGRIIITAVKDFNVKKAIGVEINDERIREALANIEKNGVTGRASIVKGNFFEVDISEATVVTMFLLTNVNEMLKPKLEKELKPGTRVVSHEFEIRGWNPKEVVKVEDGNMNHTVYLYVIGEHK-
BBG23978.1 S. tepidarius         ---MIVLSTVPYVPTPEKVVKAMLELAKTKEDDIVYDMGCGDGRIVITAVKEFNAKKAVCIEINDERIKETNSNIEKNGVVGRVSIVKGSFFEAPLSEASVLTMFLLPNVNEMLKPKLERDLKPGTRIVSHEFEMREWIPKEVIKVEDGNMNHTVYLYIIGENKG
AAY80853.1 SaciDSM 639          MTNVSYVPHVPYVPTPDKVVKRMLEIAKAGKEDTVYDLGCGDGRVVITAAKDFEVKKSVCIEINDERLKETLENINKSNVVGRAFAVKGNFFEADLSEATVLTMFLLTNVNEMLKPKLEKELKPGTRIVSHEFEIRGWIPKEVIKVEDGNMTHLVYLYIVGEHK-
ACP35686.1 Sis L.S.2.15         ---MSYVPHVPYVPTPEKVVRRMLEIAKVSQDDIVYDLGCGDGRIIITAAKDFNVKKAVGVEINDERIREALANIEKNGVTGRASIVKGNFFEVDISEATVVTMFLLTNVNEMLKPKLEKELKPGTRVVSHEFEIRGWNPKEVIKVEDGNMNHTVYLYVIGEHK-
ACP45840.1 Sis Y.G.57.14        ---MSYVPHVPYVPTPEKVVRRMLEIAKVSQDDIVYDLGCGDGRIIITAAKDFNVKKAVGVEINDERIREALANIEKNGVTGRASIVKGNFFEVDISEATVVTMFLLTNVNEMLKPKLEKELKPGTRVVSHEFEIRGWNPKEVIKVEDGNMNHTVYLYVIGEHK-
ACP48353.1 Sis Y.N.15.51        ---MSYVPHVPYVPTPEKVVRRMLEIAKVSQDDIVYDLGCGDGRIIITAAKDFNVKKAVGVEINDERIREALANIEKNGVTGRASIVKGNFFEVDISEATVVTMFLLTNVNEMLKPKLEKELKPGTRVVSHEFEIRGWNPKEVIKVEDGNMNHTVYLYVIGEHK-
ACX91839.1 SSO 98/2             ---MSYVPHVPYVPTPEKVVRRMLEIAKASQDDIVYDLGCGDGRIIITAVKDFNVKKAIGVEINDERIREALANIEKNGVTGRASIVKGNFFEVDISEATVVTMFLLTNVNEMLKPKLEKELKPGTRVVSHEFEIRGWNPKEVVKVEDGNMNHTVYLYVIGEHK-
ADX85515.1 Sis REY15A           ---MSYVPHVPYVPTPEKVVRRMLEIAKVSQDDIVYDLGCGDGRIIITAAKDFNVKKAVGVEINDERIREALANIEKNGVTGRASIVKGNFFEVDISEATVVTMFLLTNVNEMLKPKLEKELKPGTRVVSHEFEIRGWNPKEVIKVEDGNMNHTVYLYVIGEHK-
ADX82888.1 Sis HVE10/4          ---MSYVPHVPYVPTPEKVVRRMLEIAKVSQDDIVYDLGCGDGRIIITAAKDFNVKKAVGVEINDERIREALANIEKNGVTGRASIVKGNFFEVDISEATVVTMFLLTNVNEMLKPKLEKELKPGTRVVSHEFEIRGWNPKEVIKVEDGNMNHTVYLYVIGEHK-
AGE71453.1 Saci N8              ---MSYVPHVPYVPTPDKVVKRMLEIAKAGKEDTVYDLGCGDGRVVITAAKDFEVKKSVCIEINDERLKETLENINKSNVVGRAFAVKGNFFEADLSEATVLTMFLLTNVNEMLKPKLEKELKPGTRIVSHEFEIRGWIPKEVIKVEDGNMTHLVYLYIVGEHK-
AGE73726.1 Saci Ron12/I         ---MSYVPHVPYVPTPDKVVKRMLEIAKAGKEDTVYDLGCGDGRVVITAAKDFEVKKSVCIEINDERLKETLENINKSNVVGRAFAVKGNFFEADLSEATVLTMFLLTNVNEMLKPKLEKELKPGTRIVSHEFEIRGWIPKEVIKVEDGNMTHLVYLYIVGEHK-
AGJ62898.1 Sis LAL14/1          ---MSYVPHVPYVPTPEKVVRRMLEIAKVSQDDIVYDLGCGDGRIIITAAKDFNVKKAVGVEINDERIREALANIEKNGVTGRASIVKGNFFEVDISEATVVTMFLLTNVNEMLKPKLEKELKPGTRVVSHEFEIRGWNPKEVIKVEDGNMNHTVYLYVIGEHK-
AHC51757.1 Saci SUSAZ           MTNVSYVPHVPYVPTPDKVVKRMLEIAKAGKEDTVYDLGCGDGRVVITAAKDFEVKKSVCIEINDERLKETLENINKSNVVGRAFAVKGNFFEADLSEATVLTMFLLTNVNEMLKPKLEKELKPGTRIVSHEFEIRGWIPKEVIKVEDGNMTHLVYLYIVGEHK-
AOL15898.1 Sulfolobus sp.A20    ---MSYVPHVPYVPTPEKVVKRMLEIAKANQDDVVYDLGCGDGRIIITAVKDFNVKKAICIEINDERLRDTYSNIEKSGVVGRANAVKGNFFEANLSEATVVTMFLLTNVNEMLKPKLESELKPGTRIVSHEFEIRGWVPKEVIKVEDGNMNHTVYLYIIGEHK-
ARM76325.1 A. manzaensis        ---MSYVPHVPYVPTPEKVVRKMLEIAKTGPEDVVYDLGCGDGRIVIAAAKDFNAKKAICIDINDDRLKETMENIKKNGVEGKVSVEKGNFFDANLSEATVITMFLLTNVNEMLKPKLEAELKPGTRVVSHEFEMRGWTPKEVIKVEDGNMNHIVYLYIIGEHK-
AWR95980.1 A. brierleyi         ---MSYTPHVPYVPTPDKVVKKMLEIAKVGPEDVVYDLGCGDGRIVITAVKDFNAKKAVGIDINDERIQEATKNVKENGVEGKVFIRKGNFFEENISEATVVTMFLLTNVNEMLRPKLETELKPGTRVVSHEFEMRGWTPKEVVKVEDGNMNHIVYLYIGENK-
SAI84108.1 SSO                  ---MSYVPHVPYVPTPEKVVRRMLEIAKASQDDIVYDLGCGDGRIIITAVKDFNVKKAIGVEINDERIREALANIEKNGVTGRASIVKGNFFEVDISEATVVTMFLLTNVNEMLKPKLEKELKPGTRVVSHEFEIRGWNPKEVVKVEDGNMNHTVYLYVIGEHK-
WP_052846965.1 Sulfurisphaera   ---MSYIPHVPYVPTPEKVVRRMLEIANAGPEDIVYDLGCGDGRIIITAAKDFNVKKAVGIEINDERIKEALENIKRNGVENKAIVIKGNFFEIDLSEATIVTMFLLTNVNEMLKPKLEKELKPGTRVVSHEFEMRGWVPKEVIKVEDKGMTHQVYLYVIGEHK-
WP_048057696.1 M. cuprina       --------------------MKMLEIAKVGSEDVVYDLGCGDGRIIIAAVKNFGAKKAVGVDLSDERLKEAEQNAIQNGVRDKIELRKNNFLDESVSEATVITLFLLTNANELLKPKFEKELKPGTRIVSHEFEMKGWTPKEVIKVEDGNMHHLVYLYIVGEHK-
WP_126449053.1 S. acidiphilus   ---MSYIPHVPYVPTPERVVKQMLEIAKVSPGDVVYDLGCGDGRVVVTAAKDFNVKKAVGVEINDERIREVQDNIKKNGVEGRVQVIKGNFFEVDVSEATVVTMFLLTNVNEMLRPKLEKELRPGTRVISHEFEMRGWTPKQVVRVEDGNMTHTVYLYVIGENK-
WP_054836310.1 M. hakonensis    --------------------MKMLEIAKVGKEDVVFDLGCGDGRIIISAVKNFGAKKAVGVDLSDERLKEAEQNAVQNGVRDKIELRKNNFLDEDVSEATVVTLFLLTNANELLKPKFEKELKPGTRVVSHEFEMKGWKPKEVIKVEDGNMHHLVYLYIVGEHQ-
WP_110380508.1 A. sulfidivorans ---MSYVPHVPYVPTPEKVVRKMLEVAKAGPEDVVYDLGCGDGRIVIAAAKEFNVKKAICIDISDERLKETEENIKKNAVEGKVIAEKGNFFDANLSDATIVTMFLLTNVNEMLKPKLEKELKPGTRIVSHEFEMRGWTPKEVIKVEDGNMNHIVYLYIIGEHK-
WP_156006165.1 S. azoricus      ---MSYVPHVPYVPTPEKVVRKMLEIAKAGPEDIVYDLGCGDGRIIVTAAKEFHVKKAVGVEINDERIKEAIENIKRNGVEGIAHVVKGNFFEVDISEATVVTMFLLTNVNEMLMPKLQKELKPGTRIVSHEFEMRGWKPKEVVKVEDGNMTHLVYLYIVGET--
WP_054838778.1 S. metallicus     ---------------------MLELAKTKEDDVVYDMGCGDGRIVITAVKEFNAKKAVCVEINDERIKETTSNIDKNGVTGRVSIVKGSFFEAPLSEASVLTMFLLPNVNEMLKPKLERELRPGTRIVSHEFEMREWIPKEVVKVEDGNMNHTIYLYIIGENKG
```

Figure S7. Conservation of crenarchaeal vRING and lysine methyltransferase homologs. A) Alignment of vRING nuclease proteins in crenarchaeal viruses. **B)** Alignment of lysine methyltransferase homologs in the Sulfolobales. Aminoacids marked in red are important for cA_4 cleavage (A) or SAM binding (B) (Athukoralage et al. 2019, Chu et al. 2016). Residues predicted to be involved in the gp37-SiL_1451 interaction are marked in blue.

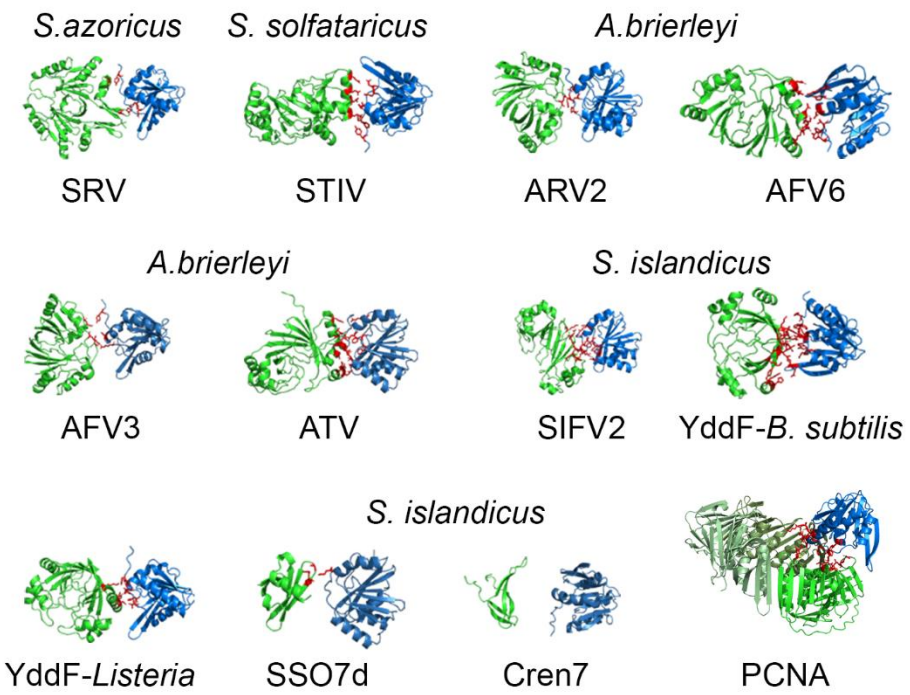

Figure S8. AlphaFold2 models of vRING nuclease proteins and their cognate lysine methyltransferase. The vRING homolog is colored in green and the lysine methyltransferase is indicated in blue. Putative interacting residues are colored in red.

A

UPREGULATED GENES

Sis REY15A	Sis LAL14/1	COG Module
SiRe_2663	SiL_2610	POORLY CHARACTERIZED
SiRe_2603	SiL_2552	POORLY CHARACTERIZED
SiRe_2464	SiL_2323	
SiRe_2463	SiL_2324	POORLY CHARACTERIZED
SiRe_2462	SiL_2325	METABOLISM
SiRe_2444	SiL_2342	POORLY CHARACTERIZED
SiRe_2381	SiL_2401	METABOLISM
SiRe_2380	SiL_2402	METABOLISM
SiRe_2250	SiL_2210	POORLY CHARACTERIZED
SiRe_2149	SiL_2114	POORLY CHARACTERIZED
SiRe_2095	SiL_2065	POORLY CHARACTERIZED
SiRe_2050	SiL_2025	INFORMATION STORAGE AND PROCESSING
SiRe_2014	SiL_1989	POORLY CHARACTERIZED
SiRe_2008	SiL_1982	CELLULAR PROCESSES AND SIGNALING
SiRe_1549	SiL_1542	POORLY CHARACTERIZED
SiRe_1536	SiL_1528	POORLY CHARACTERIZED
SiRe_1528	SiL_1520	POORLY CHARACTERIZED
SiRe_1498	SiL_1494	POORLY CHARACTERIZED
SiRe_1360	SiL_1362	CELLULAR PROCESSES AND SIGNALING
SiRe_1034	SiL_1043	METABOLISM
SiRe_1012	SiL_1021	INFORMATION STORAGE AND PROCESSING
SiRe_0981	SiL_0987	CELLULAR PROCESSES AND SIGNALING
SiRe_0978	SiL_0984	POORLY CHARACTERIZED
SiRe_0975	SiL_0981	METABOLISM
SiRe_0707	SiL_0743	METABOLISM
SiRe_0706	SiL_0742	METABOLISM
SiRe_0552	SiL_0573	METABOLISM
SiRe_0453	SiL_0492	POORLY CHARACTERIZED
SiRe_0379	NA	METABOLISM
SiRe_0374	SiL_2376	CELLULAR PROCESSES AND SIGNALING
SiRe_0318	SiL_0301	METABOLISM
SiRe_0301	SiL_0286	INFORMATION STORAGE AND PROCESSING
SiRe_0227	SiL_0220	POORLY CHARACTERIZED
SiRe_0159	SiL_0150	POORLY CHARACTERIZED
SiRe_0131	SiL_0120	CELLULAR PROCESSES AND SIGNALING
SiRe_0128	NA	INFORMATION STORAGE AND PROCESSING
SiRe_0125	NA	POORLY CHARACTERIZED
SiRe_0124	NA	CELLULAR PROCESSES AND SIGNALING
SiRe_0123	NA	CELLULAR PROCESSES AND SIGNALING
SiRe_0121	NA	CELLULAR PROCESSES AND SIGNALING

DOWNREGULATED GENES

Sis REY15A	Sis LAL14/1	COG Module
SiRe_2586	SiL_2535	METABOLISM
SiRe_2537	SiL_2486	METABOLISM
SiRe_2482	SiL_2434	METABOLISM
SiRe_2427	SiL_2356	METABOLISM
SiRe_2425	SiL_2358	METABOLISM
SiRe_2424	SiL_2359	METABOLISM
SiRe_2423	SiL_2360	POORLY CHARACTERIZED
SiRe_2422	SiL_2361	METABOLISM
SiRe_2291	SiL_2250	
SiRe_2290	NA	
SiRe_2283	SiL_2242	METABOLISM
SiRe_2123	SiL_2087	METABOLISM
SiRe_1986	SiL_1960	CELLULAR PROCESSES AND SIGNALING
SiRe_1905	SiL_1885	INFORMATION STORAGE AND PROCESSING
SiRe_1708	SiL_1702	METABOLISM
SiRe_1601	SiL_1593	METABOLISM
SiRe_1598	SiL_1590	METABOLISM
SiRe_1450	SiL_1452	POORLY CHARACTERIZED
SiRe_1449	SiL_1451	CELLULAR PROCESSES AND SIGNALING
SiRe_1427	SiL_1430	POORLY CHARACTERIZED
SiRe_1415	SiL_1418	METABOLISM
SiRe_0965	SiL_0969	CELLULAR PROCESSES AND SIGNALING
SiRe_0920	SiL_0922	POORLY CHARACTERIZED
SiRe_0789	SiL_0368	POORLY CHARACTERIZED
SiRe_0788	SiL_0369	POORLY CHARACTERIZED
SiRe_0696	SiL_0732	POORLY CHARACTERIZED
SiRe_0621	SiL_0663	POORLY CHARACTERIZED
SiRe_0594	NA	
SiRe_0593	NA	
SiRe_0592	NA	
SiRe_0591	SiL_1126	INFORMATION STORAGE AND PROCESSING
SiRe_0590	SiL_1964	INFORMATION STORAGE AND PROCESSING
SiRe_0588	SiL_0623	
SiRe_0587	SiL_0622	
SiRe_0546	SiL_0562	POORLY CHARACTERIZED
SiRe_0471	SiL_0501	METABOLISM
SiRe_0435	SiL_0470	METABOLISM
SiRe_0431	SiL_0464	CELLULAR PROCESSES AND SIGNALING
SiRe_0430	SiL_0463	METABOLISM
SiRe_0429	SiL_0462	METABOLISM
SiRe_0427	SiL_0460	POORLY CHARACTERIZED
SiRe_0072	SiL_0072	POORLY CHARACTERIZED

B

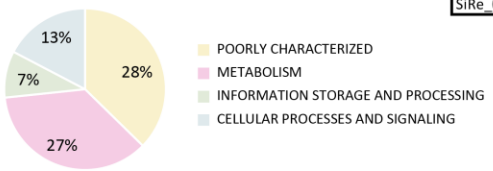

Figure S9. Differentially regulated genes in a lysine methyltransferase knock-out strain. **A)** List of differentially regulated genes in the strain *S. islandicus* REY15A Δ*sil_1451*, their corresponding homolog in *S. islandicus* LAL14/1 and their COG Module annotation. Data adapted from Chu et al. 2016. **B)** Pie chart of the COG Module functional annotation of genes in panel A.